

# Naturalness of Neutralino Dark Matter

Philipp Grothaus<sup>\*†</sup>, Manfred Lindner<sup>‡</sup> and Yasutaka Takanishi<sup>§</sup>

*Max-Planck-Institut für Kernphysik,  
Saupfercheckweg 1,  
D-69117 Heidelberg, Germany*

## Abstract

We investigate the level of fine-tuning of neutralino Dark Matter below 200 GeV in the low-energy phenomenological minimal supersymmetric Standard Model taking into account the newest results from XENON100 and the Large Hadron Collider as well as all other experimental bounds from collider physics and the cosmological abundance. We find that current and future direct Dark Matter searches significantly rule out a large area of the untuned parameter space, but solutions survive which do not increase the level of fine-tuning. As expected, the level of tuning tends to increase for lower cross-sections, but regions of resonant neutralino annihilation still allow for a band at light masses, where the fine-tuning stays small even below the current experimental limits for direct detection cross-sections. For positive values of the supersymmetric Higgs mass parameter  $\mu$  large portions of the allowed parameter space are excluded, but there still exist untuned solutions at higher neutralino masses which will essentially be ruled out if XENON1t does not observe a signal. For negative  $\mu$  untuned solutions are not much constrained by current limits of direct searches and, if the neutralino mass was found outside the resonance regions, a negative  $\mu$ -term would be favored from a fine-tuning perspective. Light stau annihilation plays an important role to fulfill the relic density condition in certain neutralino mass regions. Finally we discuss, in addition to the amount of tuning for certain regions in the neutralino mass–direct detection cross-section plane, the parameter mapping distribution if the allowed model parameter space is chosen to be scanned homogeneously (randomized).

---

<sup>\*</sup>Present address: Theoretical Particle Physics and Cosmology Group, Physics Department, Kings College London, London WC2R 2LS, U.K.

<sup>†</sup>E-mail: philipp.grothaus@kcl.ac.uk

<sup>‡</sup>E-mail: lindner@mpi-hd.mpg.de

<sup>§</sup>E-mail: yasutaka@mpi-hd.mpg.de

# 1 Introduction

Recently, the XENON100 collaboration has released new results after analyzing 225 live days of data taking. Limits on the spin-independent elastic Dark Matter-nucleon cross-section,  $\sigma^{\text{SI}}$ , have been increased by a factor of roughly four with  $2.0 \times 10^{-9}$  pb as the minimal value of the upper limit on  $\sigma^{\text{SI}}$  at a Dark Matter particle mass of 55 GeV [1]. This leads to further tests for dark matter models.

Furthermore, the ATLAS and CMS collaborations have presented their analysis of more than  $5 \text{ fb}^{-1}$  of 7 TeV, also including 8 TeV, data and claimed close to 5 local sigma level the existence of a Higgs boson with a mass of approximately 125 GeV [2, 3]. This fact fits very well to the minimal supersymmetric standard model (MSSM) because its prediction of the lightest Higgs boson mass is, when the LEP limit is taken into account, between 115 - 135 GeV depending on the supersymmetric parameters, see *e.g.* [4, 5, 6, 7, 8, 9, 10].

The existence of Dark Matter is supported by various cosmological observations such as gravitational effects on visible matter in the infrared and gravitational lensing of background radiation. Its total abundance, that has important implications for the evolution of the Universe, has been precisely measured by the WMAP collaboration [11] during the last decade. This requires that a different kind of matter beyond the Standard Model (SM) of particle physics must be postulated. One of the most popular and most intensive studied candidate is the so-called weakly interacting massive particle (WIMP) that may constitute most of the matter in the Universe. Cosmology provides therefore a good motivation for Supersymmetry (SUSY), since the MSSM possesses a natural WIMP candidate as the lightest supersymmetric particle (LSP) is stable due to  $R$ -parity conservation [12, 13] (for reviews see *e.g.* [14, 15]).

SUSY (for reviews we refer to [16, 17, 18]) has moreover the ability to solve the famous hierarchy problem by introducing superpartners with opposite spin statistics to each SM particle such that the loop contributions from superpartners cancel exactly and the weak scale is stabilized. Since SUSY must be broken, however, these cancellations are not exact and the non-discovery of SUSY particles pushes the breaking scale further up. This separation of the weak scale and of the SUSY breaking scale raises the question how easily this stability can be maintained. We apply therefore in this paper a measure of naturalness [19, 20], which was used for electroweak symmetry breaking, to the Dark Matter sector and study the level of fine-tuning.

There is a series of studies on Dark Matter in the framework of simplified variants of the MSSM, the so-called constrained MSSM (CMSSM), which possess universal supersymmetry breaking mass parameters at the grand unification scale (for example [21, 22, 23]). Due to the existence of the grand unification condition on the gaugino masses in these models, there exists a LEP limit on the lightest neutralino mass: they must be heavier than 46 GeV. According to reference [23] the lightest neutralino mass must be larger than about 200 GeV at 95 % C.L. after taking into account all relevant experimental constraints.

Instead of this restricted class of models non-universal gaugino models within the framework of the phenomenological MSSM (pMSSM) (see for example [24, 25, 26, 27, 28]) have gained much attention. In the pMSSM low-energy input parameters are used with no high-energy relations between them. These models were used to explain the possible annual modulation signals of DAMA/LIBRA [29] and CoGeNT [30] (*e.g.* [31, 32, 33, 34, 35, 36, 37, 38, 39]), as well as the excess of nuclear recoil events reported by CRESST [40]. This would be interpreted in terms of Dark Matter with a mass between roughly 10 GeV and 30 GeV and spin-independent cross-section

of order  $10^{-4} - 10^{-7}$  pb. However, it was shown that light neutralino Dark Matter scenarios consistent with DAMA/LIBRA, CoGeNT and CRESST within the pMSSM are disfavored by LHC constraints [41]. In addition there are discussions about the validity and natural consistency of these signals [42] and XENON100 [1, 43, 44] (see also [45]) as well as CDMS [46], since these experiments have excluded these “would be” Dark Matter signals anyway.

We assume therefore that Dark Matter has so far not been detected and ask how natural or fine-tuned the left-over parameter space is. Specifically we study in detail the not so well investigated neutralino mass range less than 200 GeV, taking into account all collider, cosmological and flavor constraints including the recent results of LHC Higgs researches as well as flavor studies. Over this complete mass region we find valid scenarios that may have escaped every experiment so far. We will especially show that it is possible to fulfill the muon anomalous magnetic moment condition for positive gaugino masses and a negative supersymmetric Higgs mass parameter, the  $\mu$ -term.

This article is organized as follows: in the next section, we define the fine-tuning measures and fix our notation of the neutralino sector. Then, in section 3 the method of our numerical analysis and the SUSY parameter space is discussed. Our results will be presented in section 4 including discussions about the annihilation mechanisms for neutralinos, the mapping of the level of fine-tuning into the direct detection cross-section plane, the direct detection cross-section and its dependence on the sign of the  $\mu$ -term, how the muon anomalous magnetic moment can be obtained correctly with a negative  $\mu$ -term, and lastly about functional fine-tuning and the parameter mapping distribution. Finally, we conclude in section 5.

## 2 Definition of fine-tuning

SUSY needs to be consistent with the electroweak sector of the SM and has to reproduce the correct Higgs and  $Z$ -boson masses when electroweak symmetry is spontaneously broken. The complete scalar potential reads as:

$$V = (|\mu|^2 + m_{H_u}^2)(|H_u^0|^2 + |H_u^+|^2) + (|\mu|^2 + m_{H_d}^2)(|H_d^0|^2 + |H_d^-|^2) + [b(H_u^+ H_d^- - H_u^0 H_d^0) + c.c.] + \frac{1}{8}(g^2 + g'^2)(|H_u^0|^2 + |H_u^+|^2 - |H_d^0|^2 - |H_d^-|^2)^2 + \frac{1}{2}g^2|H_u^+ H_d^{0*} + H_u^0 H_d^{-*}|^2, \quad (1)$$

where  $\mu$  is the SUSY respecting Higgs mass parameter from the superpotential,  $m_{H_u}^2$  and  $m_{H_d}^2$  mass terms of the two complex Higgs doublets  $H_u$  and  $H_d$  from the soft SUSY breaking part of the Lagrangian,  $b$  the bilinear Higgs coupling and  $g$  and  $g'$  are the  $U(1)$  and  $SU(2)$  gauge couplings, respectively. Minimizing this potential gives the well-known relation for the  $Z$ -boson mass at tree-level:

$$m_Z^2 = \frac{|m_{H_d}^2 - m_{H_u}^2|}{\sqrt{1 - \sin^2 2\beta}} - m_{H_u}^2 - m_{H_d}^2 - 2|\mu|^2, \quad (2)$$

where  $\tan \beta$  is the ratio of the vacuum expectation values (VEVs) of the two Higgs doublet fields.

From equation (2) one can immediately see that SUSY mass parameters of the order of the weak scale are preferred to avoid tuning of the  $Z$ -mass already at tree-level. To quantify this, we use the fine-tuning measure defined as the sensitivity of the  $Z$ -mass [19, 20]:

$$\Delta p_i \equiv \left| \frac{p_i}{M_Z^2} \frac{\partial M_Z^2(p_i)}{\partial p_i} \right| = \left| \frac{\partial \ln M_Z^2(p_i)}{\partial \ln p_i} \right|. \quad (3)$$

The parameters  $p_i$  that determine the  $Z$ -mass on tree-level are  $\mu$ , the two soft Higgs mass parameters ( $m_{H_u}$  and  $m_{H_d}$ ) and the bilinear coupling  $b$ . We take the total measure of fine-tuning arising from these parameters as a summation in quadrature:

$$\Delta_{\text{tot}} \equiv \sqrt{\sum_{p_i=\mu^2, b, m_{H_u}^2, m_{H_d}^2} \{\Delta p_i\}^2} , \quad (4)$$

with the individual  $\Delta p_i$ 's obtained in reference [47]

$$\Delta\mu^2 = \frac{4\mu^2}{m_Z^2} \left( 1 + \frac{m_A^2 + m_Z^2}{m_A^2} \tan^2 2\beta \right) , \quad (5)$$

$$\Delta b = \left( 1 + \frac{m_A^2}{m_Z^2} \right) \tan^2 2\beta , \quad (6)$$

$$\Delta m_{H_u}^2 = \left| \frac{1}{2} \cos 2\beta + \frac{m_A^2}{m_Z^2} \cos^2 \beta - \frac{\mu^2}{m_Z^2} \right| \left( 1 - \frac{1}{\cos 2\beta} + \frac{m_A^2 + m_Z^2}{m_A^2} \tan^2 2\beta \right) , \quad (7)$$

$$\Delta m_{H_d}^2 = \left| -\frac{1}{2} \cos 2\beta + \frac{m_A^2}{m_Z^2} \sin^2 \beta - \frac{\mu^2}{m_Z^2} \right| \left( 1 + \frac{1}{\cos 2\beta} + \frac{m_A^2 + m_Z^2}{m_A^2} \tan^2 2\beta \right) . \quad (8)$$

Here  $m_A$  denotes the pseudo-scalar Higgs mass.

The quantity  $\Delta_{\text{tot}}$  serves as an indicator how well a specific SUSY scenario avoids an unnaturally large separation of the electroweak and SUSY breaking scales. Small values are favored since they are less tuned and are therefore viewed to be more likely than those with high values of  $\Delta_{\text{tot}}$ . Note that the contributions given above do not depend on the stop mass and, hence, the fine-tuning will not show an exponential increase with the light Higgs mass. This is different to the fine-tuning measure for the pMSSM used in reference [28], or [47] who evaluated  $\Delta_{\text{tot}}$  including terms which arise at leading log level. Note that we choose our definition of the fine-tuning, since we want to avoid the dependence on a randomly chosen cut-off scale as we do not want to make any assumptions about high-energy completions. Therefore, we stick to a very rough, first estimate of the fine-tuning via a tree-level definition of  $\Delta_{\text{tot}}$ , as *e.g.* reference [26]. It is important to mention that the one-loop contribution is, however, not vanishing, from which our total measure of fine-tuning may increase by some amount.

Apart from the sensitivity of the  $Z$ -mass, a tuning of the light Higgs mass (defined analogously to equation (3)) has been discussed in reference [48]. In their set-up it has been found to be of order 100 already. Further discussions of fine-tuning in the (C)MSSM may be found in [49, 50, 51, 52].

In addition to this “parameter” fine-tuning an “equation-tuning” can appear when cancellations between different terms are a consequence of model specific relations. This will be the case for the direct detection cross-section of neutralino Dark Matter,  $\sigma^{\text{SI}}$ . To quantify this, we evaluate the sensitivity of  $\sigma^{\text{SI}}$  analogously to the  $Z$ -mass tuning and discuss its implications shortly in section 4.5. For completeness:

$$\Delta f_i \equiv \left| \frac{\partial \ln \sigma^{\text{SI}}(p_i)}{\partial \ln p_i} \right| , \quad (9)$$

with  $p_i = \{\mu, \tan \beta, M_1, M_2, m_A\}$ , see also [53].  $M_1$  is the bino and  $M_2$  the wino mass parameter. Additionally we evaluate a sensitivity of the relic abundance in section 4.6.

To fix our notation, we give some details about the neutralino  $\tilde{\chi}_1^0$  which is a mixed state of the neutral gauginos (bino  $\tilde{B}$  and neutral wino  $\tilde{W}^0$ ) and the two neutral higgsinos (down-type  $\tilde{H}_d^0$  and

up-type  $\tilde{H}_u^0$ ):

$$\tilde{\chi}_1^0 = N_{11}\tilde{B} + N_{12}\tilde{W}^0 + N_{13}\tilde{H}_d^0 + N_{14}\tilde{H}_u^0. \quad (10)$$

The coefficients  $N_{ij}$  ( $i, j = 1, 2, 3, 4$ ) are the components of the mixing matrix that diagonalizes the neutralino mass matrix:

$$M_{\tilde{N}} = \begin{pmatrix} M_1 & 0 & -M_Z \sin \theta_W \cos \beta & M_Z \sin \theta_W \sin \beta \\ 0 & M_2 & M_Z \cos \theta_W \cos \beta & -M_Z \cos \theta_W \sin \beta \\ -M_Z \sin \theta_W \cos \beta & M_Z \cos \theta_W \cos \beta & 0 & -\mu \\ M_Z \sin \theta_W \sin \beta & -M_Z \cos \theta_W \sin \beta & -\mu & 0 \end{pmatrix}. \quad (11)$$

### 3 Numerical analysis of the parameter space

As already mentioned, we study in this work the MSSM defined at the electroweak scale, the so-called pMSSM, with the eleven free parameters as in reference [54]:

$$\tan \beta, M_1, M_2, M_3, M_A, \mu, m_{\tilde{\ell}_L}, m_{\tilde{\ell}_R}, m_{\tilde{q}_{1,2}}, m_{\tilde{q}_3}, a_0, \quad (12)$$

where  $\tan \beta$  is the ratio of the VEVs of the two Higgs doublet fields,  $M_i$  ( $i = 1, 2, 3$ ) the three gauginos masses,  $m_A$  the CP-odd Higgs mass and  $\mu$  the Higgs-higgsino mass parameter. We chose different masses for left- ( $m_{\tilde{\ell}_L}$ ) and right-handed sleptons ( $m_{\tilde{\ell}_R}$ ) but no distinction in generations. Furthermore, we assume the left- and right-handed squark masses to be degenerate but different in generations ( $m_{\tilde{q}_{1,2}}$  and  $m_{\tilde{q}_3}$ ).

The trilinear terms are parameterized by  $a_0$  in the following way:

$$A_t = a_0 Y_t m_{\tilde{q}_3}, \quad A_b = a_0 Y_b m_{\tilde{q}_3}, \quad A_\tau = a_0 Y_\tau \sqrt{m_{\tilde{\ell}_L} m_{\tilde{\ell}_R}}. \quad (13)$$

This implies that we use non-zero trilinear couplings that are proportional to the third generation squark masses for  $A_t$  and  $A_b$ , not as in reference [54], and the geometric mean of the slepton masses for the leptonic trilinear term. Since the SM Yukawa couplings of the first two generations are known to be very small, we can safely neglect  $A_u, A_d, A_e$ , *i.e.* we set them to zero.

In order to calculate the level of tuning, the parameters of equation (12) are randomly varied in the following ranges:

$$\begin{aligned} M_1 &\in [10, 200] \text{ GeV}, & M_2 &\in [100, 2000] \text{ GeV}, & M_3 &\in [100, 4000] \text{ GeV}, \\ m_A &\in [90, 4000] \text{ GeV}, & |\mu| &\in [90, 2000] \text{ GeV}, & a_0 &\in [-4.0, 4.0], \\ m_{\tilde{q}_{1,2}} &\in [400, 4000] \text{ GeV}, & m_{\tilde{q}_3} &\in [200, 4000] \text{ GeV}, & \tan \beta &\in [2, 65], \\ m_{\tilde{\ell}_L} &\in [100, 4000] \text{ GeV}, & m_{\tilde{\ell}_R} &\in [60, 4000] \text{ GeV}. \end{aligned}$$

For every simulated scenario we create a different random number  $\lambda$  for each of the eleven input parameters  $x$  using Mersenne Twister [55, 56]. Their values are then given by  $x = x_{\min} + \lambda(x_{\max} - x_{\min})$ , where  $x_{\min/\max}$  is the minimal/maximal value of  $x$ , respectively, and forwarded to **SuSpect**. In order to save memory and make the scan more efficient, we immediately remove all the scenarios that do not respect the experimental ranges listed in table 1. In this way we create four sets of simulated data: two sets for each sign of  $\mu$ , one excluding, one including the measurement of the muon anomalous magnetic moment  $a_\mu$ . Excluding  $a_\mu$  from the applied cuts, we get a total

Quantity		Reference(s)
$\Omega h^2$	[0.089, 0.136]	[11]
$m_h$	(121.0, 129.0) GeV	[2, 3, 58, 59, 60, 61, 62, 63]
$\text{Br}(B \rightarrow s\gamma)$	$[2.89, 4.21] \times 10^{-4}$	[64]
$\text{Br}(B_s \rightarrow \mu^+\mu^-)$	$< 4.5 \times 10^{-9}$	[65]
$\text{Br}(B_u \rightarrow \tau\bar{\nu})$	$0.52 < R_{B\tau\nu} < 2.61$	[66]
$\text{Br}(K \rightarrow \mu\nu)$	$0.985 < R_{l23} < 1.013$	[67]
$a_\mu$	$[0.34, 4.81] \times 10^{-9}$	[68]
$\Gamma(Z \rightarrow \tilde{\chi}_1\tilde{\chi}_1)$	$< 3$ MeV	[69]
$\sigma(ee \rightarrow \tilde{\chi}_1\tilde{\chi}_{2,3})$	$< 100$ fb	[69]
$\Delta\rho$	$< 0.002$	[69]

Table 1: The experimental constraints.

number of approximately 372800 (246800) scenarios for positive (negative)  $\mu$ . The data sets that include that constraint consist of 178000 (64000) scenarios.

We emphasize that we have studied not only the case  $\mu > 0$  but also  $\mu < 0$  which will turn out to be important. One might wonder if we can manage to satisfy the limit of the muon anomalous magnetic moment with a negative  $\mu$ -term. This issue will be discussed later in section 4.4.

For our analysis we take into account different experimental data from cosmology, flavor and collider physics. The Dark Matter abundance constraints arise from the WMAP analysis [11] of the determination of the relic density. We set the neutralino relic density,  $\Omega h^2$ , within the  $2\sigma$  range [57]  $\Omega h^2 \in [0.089, 0.136]$ , where experimental and theoretical uncertainties are included. The influence of the direct detection search – XENON100 (2012) – of Dark Matter will be explicitly shown in the plots representing our results. Results of ATLAS and CMS analyses for a standard model-like Higgs boson mass [2, 3, 58, 59, 60, 61, 62, 63] provide the allowed mass limit:  $121.0 \text{ GeV} < m_h < 129.0 \text{ GeV}$ . Since the recent results of both collaborations are still preliminary, we take the range not too restrictive. A smaller mass range would not affect our results except that the numerical simulations would be more time-consuming. Also the light gluino mass and light squark masses of the first two generations are excluded by the analyses of the signature of missing transverse energy [70, 71], see also [72, 73], so we allow their masses to be greater than 800 GeV and 1 TeV, respectively.

We also take into account the constraint coming from pseudo-Higgs boson searches [74, 75] that have excluded a significant fraction of the  $M_A - \tan\beta$  plane at small  $M_A$  and large values of  $\tan\beta$ . Moreover, LEP constraints are included in our study: the invisible  $Z$ -decay width  $\Gamma(Z \rightarrow \tilde{\chi}_1\tilde{\chi}_1) < 3$  MeV [69], the pair production cross-section  $\sigma(ee \rightarrow \tilde{\chi}_1\tilde{\chi}_{2,3}) < 100$  fb [76],  $\Delta\rho < 0.002$  [77] and the mass limits of supersymmetric particles [69, 77].

The experimental constraints including flavor and collider physics applied in our analyses are listed in table 1, where  $R_{B\tau\nu}$  is the ratio between the SUSY and SM prediction of the branching ratio  $\text{Br}(B_u \rightarrow \tau\bar{\nu})$ ,  $R_{l23}$  the leptonic kaon decay quantity and  $a_\mu$  the muon anomalous magnetic moment. For the latter quantity we use the  $3\sigma$  range [68], because there are theoretical uncertainties about hadronic effects.

The supersymmetric spectrum is obtained by `SuSpect` [78] using the default SUSY breaking scale, the neutralino relic density  $\Omega h^2$ , the spin-independent cross-section with protons  $\sigma^{\text{SI}}$  and the annihilation channels were calculated by the `micrOMEGAs` code [79, 80], while the low-energy observables

( $\text{Br}(B \rightarrow s\gamma)$ ,  $\text{Br}(B_s \rightarrow \mu^+\mu^-)$ ,  $R_{B\tau\nu}$ ,  $R_{l23}$ ) and  $a_\mu$  have been determined by `SuperIso` [81].

In our analysis we use the following values of the quark form-factors in the nucleon which are the default values in the `micrOMEGAs` package:

$$\begin{aligned} f_d^p &= 0.033, & f_u^p &= 0.023, & f_s^p &= 0.26, \\ f_d^n &= 0.042, & f_u^n &= 0.018, & f_s^n &= 0.26. \end{aligned} \tag{14}$$

It should be mentioned that the main uncertainty comes from the strange quark coefficient, and using another set of quark coefficients (the large corrections to  $f_s^{p/n}$ ) can lead to a shift by a factor 2 – 6 in the spin independent cross-section [82].

Note that we do not calculate a  $\chi^2$  as a probability measure in this work but see every scenario that passes the constraints as equally probable. Only the envelope of our final plots, that mildly depends on the parameters, has a meaning: The area outside of it can never be reached with the chosen parameter space. We take the viewpoint that tuned scenarios are less likely to form valid models of the pMSSM.

## 4 Results

### 4.1 Obtaining the correct relic density

First we discuss the different mechanisms that bring the relic density into the cosmological interesting region. The relic density is basically set by the thermally averaged annihilation cross-section,  $\langle\sigma_{ann}v\rangle$ , using a freeze-out mechanism. In figure 1 we plot the relic density on a log scale versus the neutralino mass as obtained by our simulation with `micrOMEGAs` (for simplicity we plot here  $\Omega h^2 < 0.2$ ), where the most important annihilation channels are presented by the indicated color code. In general a very efficient mechanism is needed to end up with a high enough  $\langle\sigma_{ann}v\rangle$  to obtain the correct relic abundance.

Lepton final states (dark-blue points in figure 1) are the most dominant annihilation channels and are present in our complete neutralino mass range. To obtain these a distinction of left- and right-handed slepton masses is necessary as we will discuss later. In past studies of the pMSSM the importance of light stau annihilations at neutralino masses between 60 and 80 GeV has not clearly been pointed out, compare [21, 26, 28] for past scans.

The two resonant  $Z$ - and light Higgs-boson annihilations can easily be seen at around 40 and 60 GeV (red points), respectively. Above a mass of roughly 80 GeV the neutralino may annihilate into two  $W$ -bosons (light-blue). There are further scenarios with dominant annihilations into light quarks for  $m_{\tilde{\chi}} \gtrsim 80$  GeV hidden behind the lepton final states. The lower branch (dark-green) corresponds to chargino coannihilations, but for our chosen range of the lightest neutralino mass this mechanism is too efficient and never produces enough Dark Matter. These coannihilations are therefore unimportant for our further discussion, as we are also taking into account the lower bound from the WMAP measurement. On the other hand, slepton coannihilations will play an important role at neutralino masses above 90 GeV (light-green). They are accompanied by a region of top final states at approximately 180 GeV (orange).

When mapping the different models with their mechanisms into the  $m_{\tilde{\chi}} - \sigma^{\text{SI}}$  plane, we find a rather well ordered picture (all constraints except the muon anomalous magnetic moment have been

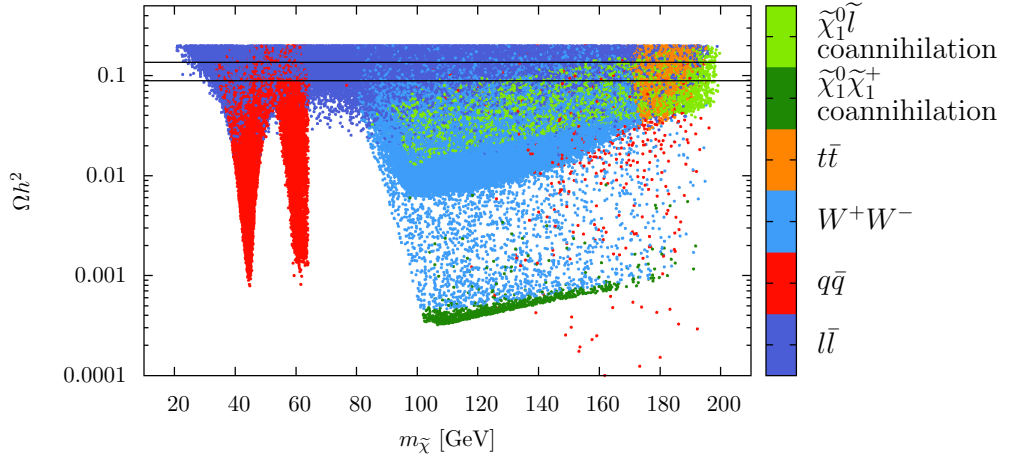


Figure 1: The relic density and the different (co)annihilation mechanisms presented for negative  $\mu$  (see color coding and table 2 for more information about the final states). We have applied all collider and flavor constraints. The black lines show the upper and lower bounds that will be applied on the relic density;  $\Omega h^2 \in [0.089, 0.136]$ . Here  $q\bar{q}$  stands for a light quark and  $\ell\bar{\ell}$  for a lepton pair. The plot is similar for positive  $\mu$ .

	initial state	final states
chargino coannihilation	$\tilde{\chi}_1^0 \tilde{\chi}_1^+$	$sc, ud, tb, e\nu_e, \mu\nu_\mu, ZW$
slepton coannihilation	$\tilde{\chi}_1^0 \tilde{\tau}_1$	$\gamma\tau, \tau h, W\nu_\tau, Z\tau$
	$\tilde{\chi}_1^0 \tilde{e}_R$	$\gamma e$
	$\tilde{\chi}_1^0 \tilde{\nu}_\tau$	$W\tau, Z\nu_\tau, \nu_\tau h$
	$\tilde{\chi}_1^0 \tilde{\nu}_e$	$W e, Z\nu_e$

Table 2: List of the dominant annihilation channels as obtained by our simulation.

applied). We show the case of a negative  $\mu$ -term in figure 2.

The quark final states at neutralino masses between 40 and 60 GeV are due to the  $s$ -channel  $Z$ -boson and light Higgs boson,  $h$ , resonances. The chargino mediated  $t$ -channel and neutral Higgs mediated  $s$ -channel annihilations into  $W$ -bosons fill a band at  $\sigma^{\text{SI}} \simeq 10^{-9}$  pb (light-blue). In this region (red points above 80 GeV) one also finds quark final states via heavy neutral Higgs,  $H$ , and CP-odd Higgs,  $A$ , exchanges. The most prominent mechanism, the annihilation into a pair of leptons, is homogeneously distributed and mainly mediated through  $t$ -channel light stau or  $s$ -channel  $Z$ ,  $h$ ,  $A$ ,  $H$  exchange and their interference terms. Slepton coannihilations are situated in an area below the  $W$ -bosons final states. The chargino coannihilations are not present as argued above<sup>1</sup>.

<sup>1</sup>Some scenarios of chargino coannihilations have been present even after cutting the relic density, however, these were extremely rare (of order 0.02%) and we removed them from our study.



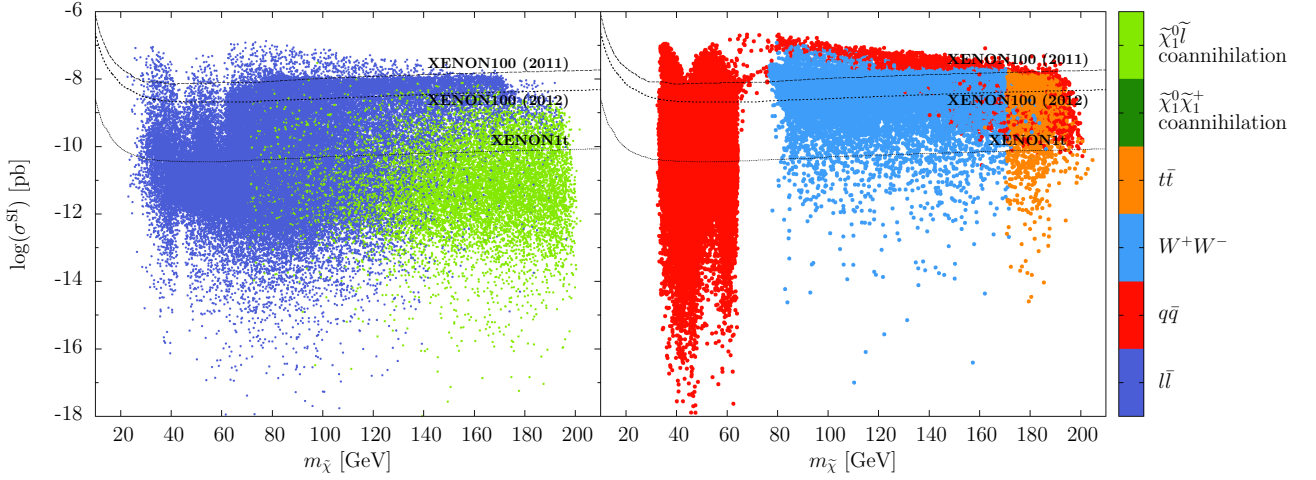


Figure 2: Dominant contribution to the neutralino annihilation in the  $m_{\tilde{\chi}} - \sigma^{\text{SI}}$  plane for negative  $\mu$ . The required relic density and all collider physics constraints have been applied except the anomalous magnetic moment of the muon. Here  $q\bar{q}$  stands for a light quark and  $\ell\bar{\ell}$  for a lepton pair. For better visibility we display the results in two figures.

The arrangement of the decay mechanisms holds generally and shows, aside from a different scale of the direct detection cross-section, no difference between positive and negative  $\mu$  (for more details see figure 3).

Note that we have calculated the annihilation cross-sections of two Dark Matter into two photons in our models that satisfy all experimental constraints except the muon anomalous magnetic moment, and we found that the order of  $\langle\sigma_{\tilde{\chi}\tilde{\chi}\rightarrow\gamma\gamma}v\rangle$  is far below the recent claim of a gamma-ray line in the

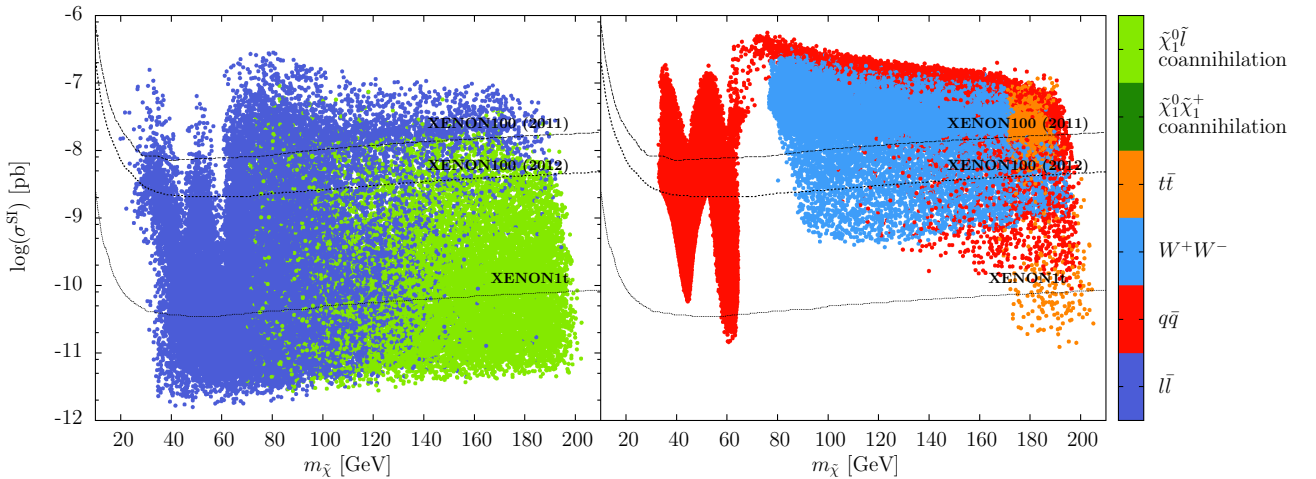


Figure 3: Dominant contribution to the neutralino annihilation in the  $m_{\tilde{\chi}} - \sigma^{\text{SI}}$  plane for a positive  $\mu$  in analogy to figure 2.

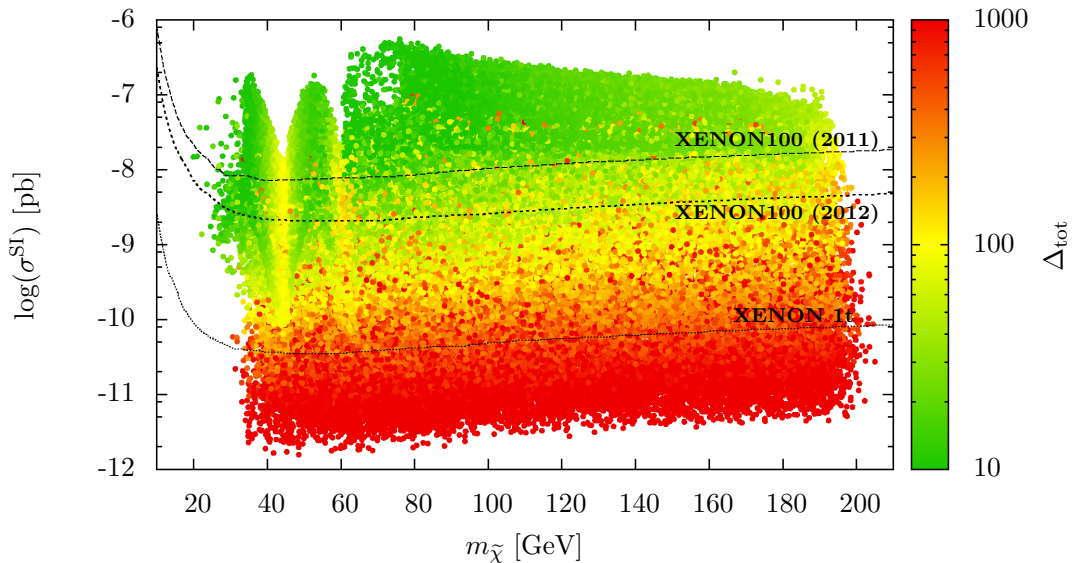


Figure 4: The level of fine-tuning for our models in the  $m_{\tilde{\chi}} - \sigma^{\text{SI}}$  plane. The colored points show the fine-tuning  $\Delta_{\text{tot}}$  for some specific parameter combination. Points with  $\Delta_{\text{tot}} < 10$  are given the value 10 and  $\Delta_{\text{tot}} > 1000$  the value 1000. The lines represent the exclusion limits of XENON100 (2011) and XENON100 (2012), and the prediction for XENON1t, respectively.

Fermi-LAT data [83]. Thus, we conclude that a dark matter particle mass of order 130 GeV and a partial annihilation cross-section into two photons of approximately  $1.3 \times 10^{-27} \text{cm}^3 \text{s}^{-1}$  is not compatible with our models.

## 4.2 Fine-tuning and the spin-independent elastic WIMP nucleon cross-section

We will discuss the spin-independent elastic WIMP nucleon cross-section as function of the neutralino mass with respect to the fine-tuning measure, equation (4). In this section, we show our results applying all experimental constraints discussed above except the muon anomalous magnetic moment. To stress its impact we will consider this quantity separately in section 4.4.

First, positive values of the  $\mu$ -term will be presented: In figure 4 low fine-tuned regions can be found near the  $Z$ - and  $h$ -resonances down to  $10^{-10}$  pb and for  $\sigma^{\text{SI}} \gtrsim 10^{-8}$  pb at masses above 80 GeV. A great part of the latter region is already excluded by the current XENON limit, so that low fine-tuned Dark Matter preferably appears for positive  $\mu$  at masses between 20 and 60 GeV. Moving towards the exact  $Z$ -resonance a rise in  $\Delta_{\text{tot}}$  can be observed, which can be understood as follows: In order to obtain the correct relic density the neutralino-neutralino- $Z$ -coupling has to be decreased to compensate for the resonant enhancement of  $\langle \sigma_{\text{ann}} v \rangle$ . This coupling is determined by

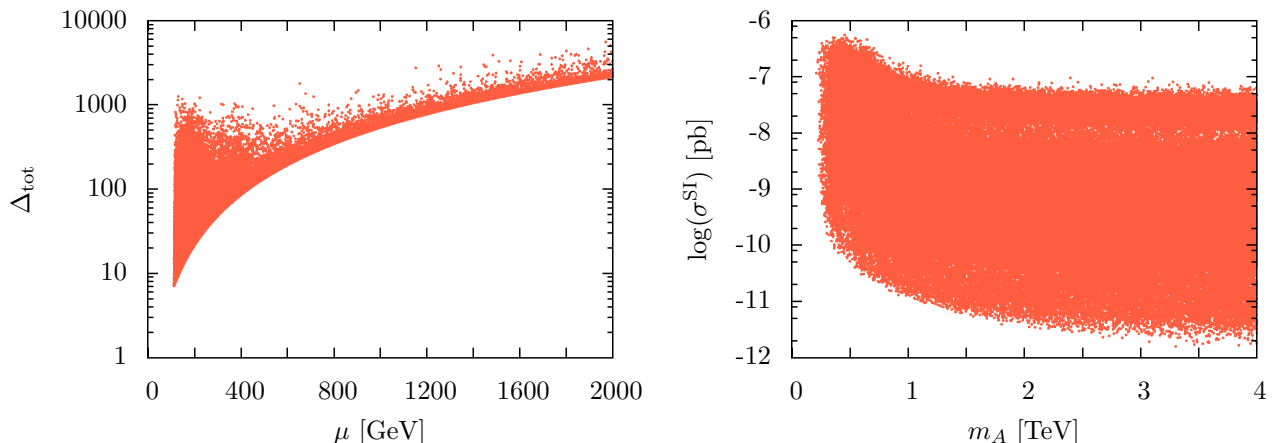


Figure 5: Plots motivating our upper bounds on the  $\mu$ -term (left panel) and  $m_A$  (right panel). The strong increase of the minimal amount of fine-tuning with  $\mu$  and the negligible decrease of  $\sigma^{\text{SI}}$  with  $m_A$  are visible. They are shown for a positive  $\mu$ -term but are similar for negative values.

the higgsino components of the neutralino [84]:

$$\langle \sigma_{ann} v \rangle \propto |C_A^{\tilde{\chi}\tilde{\chi}Z}|^2 \propto (N_{14}^2 - N_{13}^2)^2 . \quad (15)$$

Increasing  $\mu$  decreases  $C_A^{\tilde{\chi}_1^0 \tilde{\chi}_1^0 Z}$  (see equations (25) and (26)) and reproduces the correct relic abundance close to the exact resonance but at the same time increases the fine-tuning (compare the left panel of figure 5). Note that at the  $Z$ -resonance  $\mu$ -term is fixed due to the relic density condition and the fine-tuning stays roughly constant when moving towards lower direct detection cross-sections.

Highly fine-tuned models appearing in figure 4 in the otherwise low fine-tuned regions show a small  $\tan\beta$  and a large  $m_A$ . In that case  $\Delta b$ , equation (6), becomes very large.

The models lying out of the  $Z$ - and  $h$ -resonances show a clear tendency towards higher fine-tuning for smaller  $\sigma^{\text{SI}}$  (see also [53]). To decrease  $\sigma^{\text{SI}}$ , the higgsino component of the neutralino needs to be reduced which in turn is achieved through increasing the  $\mu$ -term. Away from the  $Z$ - and  $h$ -resonances a small neutralino-proton cross-section can therefore for positive  $\mu$  only be obtained at the cost of higher fine-tuning. To decrease further  $\sigma^{\text{SI}}$  one could, in principle, increase  $\mu$  above 2 TeV and  $m_A$  above 4 TeV, but the effect on  $\sigma^{\text{SI}}$  is small and the fine-tuning becomes unacceptably large (see figure 5).

Now, we will turn to negative values of the  $\mu$ -term (see figure 6). The big difference is that the parameter region has just begun to be probed by direct detection experiments. Compared to a positive  $\mu$ -term the neutralino-proton cross-section is shifted to smaller values, so that every mass-region still offers models that explain the Dark Matter riddle with low electroweak fine-tuning. These shifts due to cancellations between light and heavy Higgs contributions to  $\sigma^{\text{SI}}$  are possible for specific combinations of the input parameters, preferably when the absolute value of  $\mu$  is small, and will be discussed more detailed in section 4.3. In this way, an interesting region occurs for light Dark Matter near the  $Z$ - and  $h$ -resonances where the fine-tuning stays small even if  $\sigma^{\text{SI}}$  is decreased to tiny values.

Across the complete neutralino mass region, scenarios with large fine-tuning show up at  $\sigma^{\text{SI}} \approx$

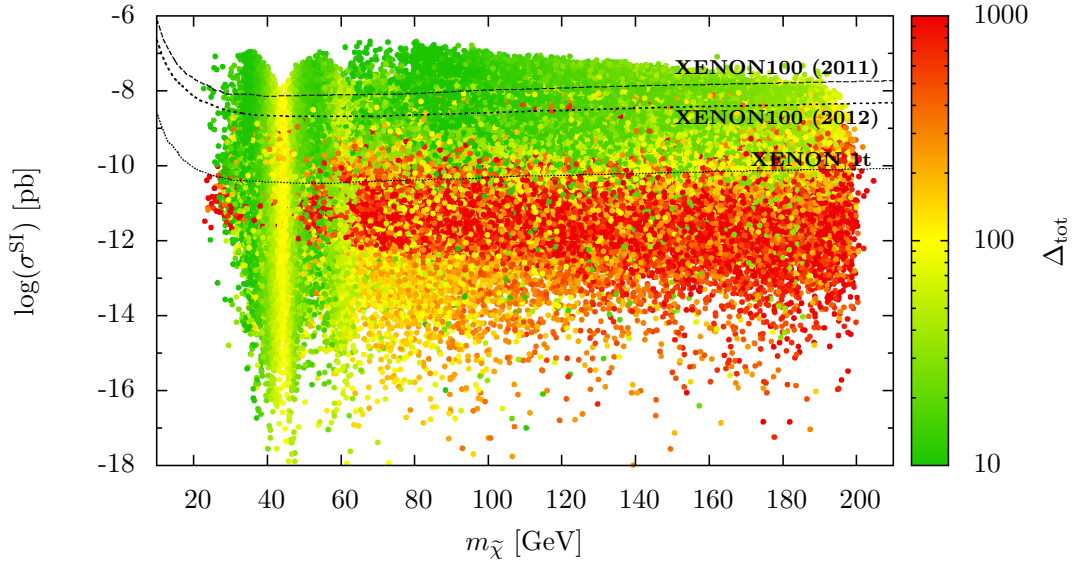


Figure 6: The level of fine-tuning for a negative  $\mu$ -term in analogy to figure 4.

$10^{-11}$  pb below the expected XENON1t “exclusion line”. These come from light stau mediated annihilations whose stau mass is strongly influenced by the off-diagonal elements of the slepton mass matrix (see figures 2 and 7). The stau masses are given by:

$$m_{\tilde{\tau}_{1,2}}^2 = \frac{1}{2} \left[ m_{\tilde{l}_L}^2 + m_{\tilde{l}_R}^2 - \frac{1}{2} M_Z^2 \cos 2\beta + 2m_\tau^2 \pm \sqrt{\left( m_{\tilde{l}_L}^2 - m_{\tilde{l}_R}^2 + \left(-\frac{1}{2} + 2\sin^2 \theta_W\right) M_Z^2 \cos 2\beta \right)^2 + 4m_\tau^2 (A_\tau - \mu \tan \beta)^2} \right]. \quad (16)$$

There are two ways to get light stau masses: (i)  $m_{\tilde{l}_L} \sim m_{\tilde{l}_R}$  and (ii)  $m_{\tilde{l}_L} \gg m_{\tilde{l}_R}$ . In the first case we can approximate  $m_{\tilde{\tau}_1}^2$  as:

$$m_{\tilde{\tau}_1}^2 \approx m_{\tilde{l}_R}^2 + \frac{1}{4} M_Z^2 - |m_\tau (A_\tau - \mu \tan \beta)| \approx \frac{5}{4} M_Z^2 - |m_\tau (A_\tau - \mu \tan \beta)|, \quad (17)$$

where we used  $-\frac{1}{2} + 2\sin^2 \theta_W \simeq 0$  and assumed in the last step  $m_{\tilde{l}_R} \sim M_Z$ . If a large  $\mu$ -term is present the  $\tilde{\tau}_1$  mass can be suppressed (even below 100 GeV) when  $(A_\tau - \mu \tan \beta) \approx \frac{M_Z^2}{m_\tau} \approx 10^4$  GeV. The same is true for the second case. As an approximation for the stau masses we find here:

$$m_{\tilde{\tau}_1}^2 \approx m_{\tilde{l}_R}^2 + \frac{M_Z^2}{4} - \frac{m_\tau^2 (A_\tau - \mu \tan \beta)^2}{16m_{\tilde{l}_L}^2}. \quad (18)$$

One can see that the stau mass is primarily determined by  $m_{\tilde{l}_R}$  and for  $\frac{m_\tau^2 (A_\tau - \mu \tan \beta)^2}{16m_{\tilde{l}_L}^2} \sim 100^2$  GeV<sup>2</sup> the mass is suppressed by the off-diagonal elements. This explains why the models with the lightest possible staus are severely fine-tuned.

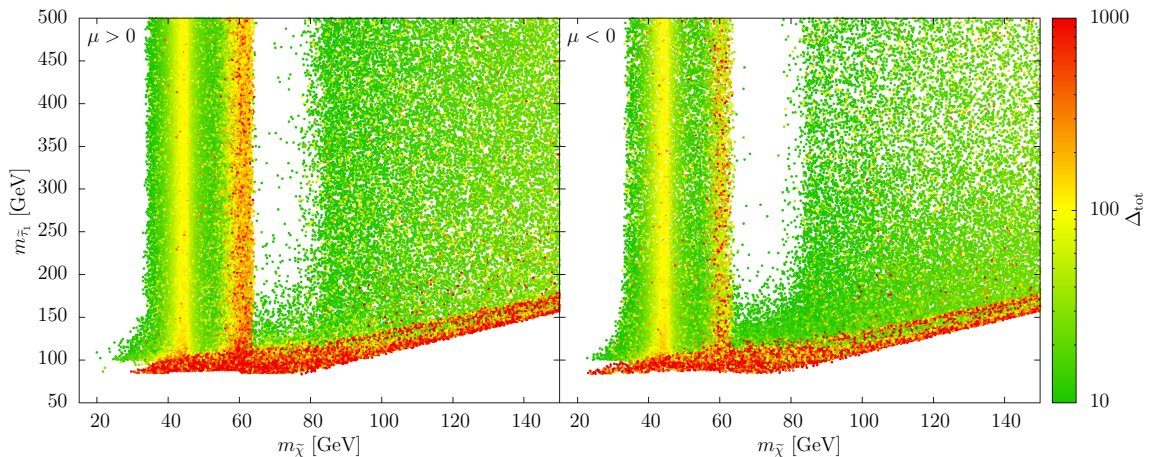


Figure 7: Models with very light staus and their level of fine-tuning. We show the cases for a positive (left) and negative (right)  $\mu$ -term separately.

In figure 7 one can also see that in the neutralino mass region  $m_{\tilde{\chi}} \approx [60, 80]$  GeV exclusively light staus are present. Here, light stau annihilation is the only possible mechanism to obtain the correct relic abundance. For these scenarios we find that the second case, *i.e.*  $m_{\tilde{l}_L} \gg m_{\tilde{l}_R}$ , is dominant to produce small  $m_{\tilde{\tau}_1}$ .

Below neutralino masses of around 35 GeV we find for both signs of  $\mu$  a separation of high and low fine-tuned models. Scenarios with a small  $\mu$ -term, *i.e.* small fine-tuning, possess a significant higgsino component so that next to the slepton annihilation an annihilation via the  $Z$ -boson and their interference term is dominant for  $\langle \sigma_{ann} v \rangle$ . For the points with  $m_{\tilde{\tau}_1} < 100$  GeV only stau mediated neutralino annihilation is important and we find that  $m_{\tilde{l}_L} \sim m_{\tilde{l}_R}$ . A detailed study on light staus may be found in reference [54].

At the  $h$ -resonance,  $m_{\tilde{\chi}} \sim 60$  GeV, one can find scenarios with high fine-tuning at  $\sigma^{\text{SI}} \approx 10^{-10}$  pb above the XENON1t “exclusion limit” (see figure 6). In contrast to the  $Z$ -boson resonance, the  $\mu$ -term for  $h$ -resonant neutralino annihilation is not fixed through the relic density condition, because the Higgs-fermion-fermion coupling is dependent on a SUSY parameter; in the case for annihilation into  $b\bar{b}$  the coupling constant is proportional to  $\cos\beta$ . Models that have a small value of  $\tan\beta$ , *i.e.* a rather large  $\cos\beta$  and, hence, a large Higgs- $b\bar{b}$ -coupling, need a high  $\mu$ -term to decrease the neutralino-neutralino-Higgs coupling in order to keep the overall neutralino annihilation rate fixed at the value that reproduces the correct relic density. Despite their tiny higgsino component their direct detection cross-section,  $\sigma^{\text{SI}}$ , is not minimal. See section 4.3 for further discussions on this. (These models can also be found in the vertical red stripe at 60 GeV in figure 7.)

Note that the LHC phenomenology of the neutralino mass range under 70 GeV has been studied in reference [85]. They find that the invisible  $h$  decay width may exclude parameter regions of small  $\mu$  and  $M_1$ . Taking the most conservative upper bound of  $\text{BR}_{\text{inv}} < 0.65$  they present how this constraint cuts into the low fine-tuned regions for a positive  $\mu$ -term. The implications on our study are not significant. Besides, for a negative  $\mu$ -term the constraints are not competitive at all.

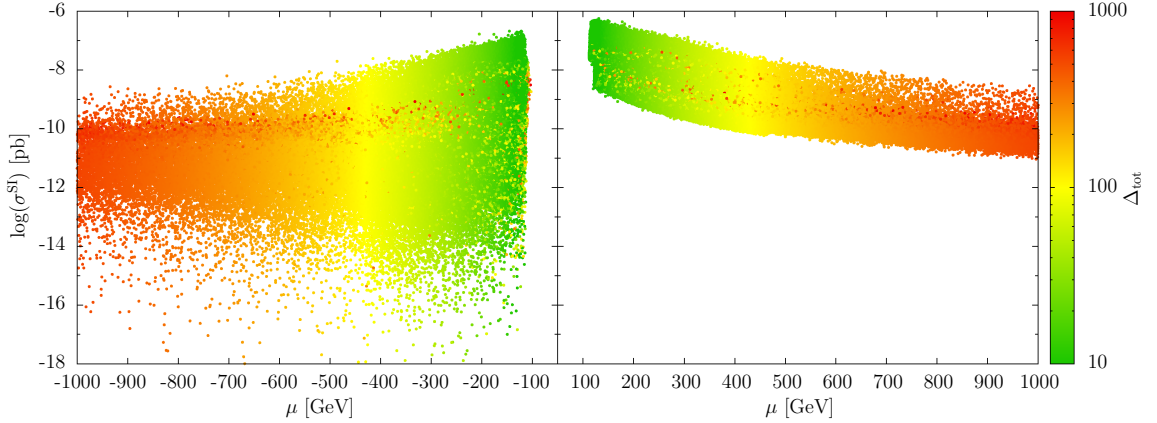


Figure 8: The level of fine-tuning and the direct detection cross-section for negative (left) and positive (right) values of  $\mu$ .

### 4.3 The direct detection cross-section and the $\mu$ -term

From figure 8, one can immediately notice a clear difference for the spin-independent neutralino proton cross-section when the sign of  $\mu$  is flipped. A negative value allows for much lower cross-sections for a given absolute value of  $\mu$  than a positive sign. We want to point out again, that the red points showing up at small absolute values of  $\mu$  have a large  $m_A$  and a small  $\tan\beta$ .

Let us discuss in detail why the sign of the  $\mu$ -term plays an important role for the SI cross-section calculation. The dominating terms in the SI cross-section come from  $t$ -channel light and heavy Higgs boson exchanges. The formula can be found in references [14, 86, 87]:

$$\sigma^{\text{SI}} \simeq \frac{8G_F^2}{\pi} M_Z^2 m_{\text{red}}^2 \left[ \frac{F_h I_h}{m_h^2} + \frac{F_H I_H}{m_H^2} \right]^2, \quad (19)$$

where  $G_F$  is Fermi constant and  $m_{\text{red}}$  is the neutralino-nucleon reduced mass:

$$m_{\text{red}} \equiv \frac{m_{\tilde{\chi}_1^0} m_N}{m_{\tilde{\chi}_1^0} + m_N}. \quad (20)$$

The functions  $F_{h,H}$  and  $I_{h,H}$  are defined as follows

$$F_h \equiv (-N_{11} \sin \theta_W + N_{12} \cos \theta_W) (N_{13} \sin \alpha + N_{14} \cos \alpha), \quad (21)$$

$$F_H \equiv (-N_{11} \sin \theta_W + N_{12} \cos \theta_W) (N_{13} \cos \alpha - N_{14} \sin \alpha), \quad (22)$$

$$I_{h,H} \equiv \sum_q k_q^{h,H} m_q \langle N | \bar{q}q | N \rangle. \quad (23)$$

The angle  $\alpha$  is the mixing of the mass eigenstates ( $h$  and  $H$ ), and the coefficients  $k_q^{h,H}$  are given by

$$\begin{aligned} k_{u\text{-type}}^h &= \cos \alpha / \sin \beta, & k_{d\text{-type}}^h &= -\sin \alpha / \cos \beta, \\ k_{u\text{-type}}^H &= -\sin \alpha / \sin \beta, & k_{d\text{-type}}^H &= -\cos \alpha / \cos \beta, \end{aligned}$$

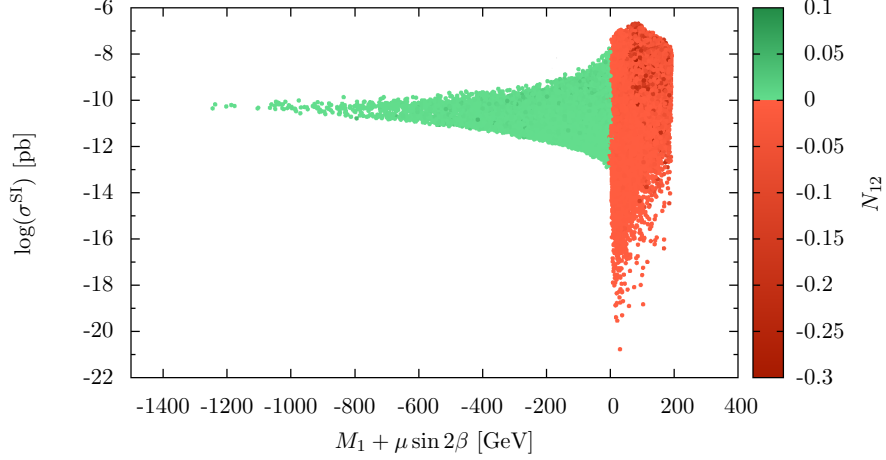


Figure 9: The dependence of  $\sigma^{\text{SI}}$  as a function of the quantity  $M_1 + \mu \sin 2\beta$  and the wino component ( $N_{12}$ ) as obtained by our simulations.

for the up-type and down-type quarks, respectively. We neglect threshold corrections for simplicity in our discussion.

To find a good approximation for the elements of the neutralino mixing matrix, we use the large SUSY scale approximation  $(M_i \pm |\mu|)^2 \gg M_Z^2$  ( $i = 1, 2$ ) from reference [88] and find for the components:

$$N_{12} \simeq -M_Z^2 \cos \theta_W \sin \theta_W \frac{M_1 + \mu \sin 2\beta}{(M_1 - M_2)(M_1^2 - \mu^2)} , \quad (24)$$

$$N_{13} \simeq -M_Z \sin \theta_W \frac{M_1 \cos \beta + \mu \sin \beta}{M_1^2 - \mu^2} , \quad (25)$$

$$N_{14} \simeq M_Z \sin \theta_W \frac{M_1 \sin \beta + \mu \cos \beta}{M_1^2 - \mu^2} . \quad (26)$$

The unitary condition on the mixing angles yields

$$N_{11} = \sqrt{1 - N_{12}^2 - N_{13}^2 - N_{14}^2} . \quad (27)$$

These approximations are in good agreement with the simulations. The only strong deviation occurs for scenarios with a dominant annihilation into  $W$ -bosons near neutralino masses of around 80 GeV. For all other annihilation mechanisms they give sufficient precision for a reliable qualitative discussion. Evaluating the complete expression in the decoupling limit<sup>2</sup> yields the following formula:

$$\sigma^{\text{SI}} \simeq \frac{8G_F^2 m_{\text{red}}^2}{\pi} \frac{M_Z^4 \sin^2 \theta_W}{(M_1^2 - \mu^2)^2} \left[ \frac{I_H}{m_H^2} \mu \cos 2\beta + \frac{I_h}{m_h^2} (M_1 + \mu \sin 2\beta) \right]^2 (N_{11} \sin \theta_W - N_{12} \cos \theta_W)^2 . \quad (28)$$

<sup>2</sup>*I.e.* we use  $\sin^2(\alpha - \beta) \simeq 1$ , such that  $\sin \alpha \simeq \cos \beta$ ,  $\cos \alpha \simeq -\sin \beta$ .

Note, that  $\cos 2\beta$  is negative, *i.e.*  $\cos 2\beta \approx -1$  ( $\tan \beta > 2$ ), such that both contributions within the square brackets seem to have a different sign. However, looking at the  $k$ -coefficients one can see that  $I_h$  and  $I_H$  preferably have opposite signs in the decoupling limit, such that both terms actually add up for a positive  $\mu$ -term.

On the contrary, if  $\mu$  is negative, cancellations between both terms within the square brackets are possible and  $\sigma^{\text{SI}}$  can be significantly smaller. However, this is only correct when  $M_1 + \mu \sin 2\beta$  is positive. Note that in this case the wino component, equation (24), is negative since  $M_2 > M_1$  and  $|\mu| > M_1$  for the great majority of our models (see figure 9). The boundary at  $M_1 + \mu \sin 2\beta \approx 200$  GeV occurs for the maximal values of  $M_1$  and  $\tan \beta$  when, at the same time,  $|\mu|$  is small.

For  $M_1 + \mu \sin 2\beta < 0$  a cancellation is no longer possible and the resulting  $\sigma^{\text{SI}}$  is higher. Most of the scenarios with a positive wino component in figure 9 correspond to the earlier mentioned highly fine-tuned models at the Higgs-resonance. These showed large absolute values of the  $\mu$ -term and small  $\tan \beta$ . Then,  $M_1 + \mu \sin 2\beta$  takes the smallest possible negative values and the cross-section is rather high (*i.e.*  $10^{-10}$  pb). Also, those scenarios with light staus whose mass is suppressed by the off-diagonal mass matrix elements possess a positive wino component and hence map accordingly into the direct detection plane.

An expression similar to equation (28) has been found in [89], however the wino component has not been considered there. Even though cancellations that occur between  $N_{11}$  and  $N_{12}$  may be neglected, since the bino component is in general much larger than the wino component, the sign of  $N_{12}$  is crucial for the behavior of  $\sigma^{\text{SI}}$ .

#### 4.4 The muon anomalous magnetic moment and the $\mu$ -term

In figure 10 we applied the muon anomalous magnetic moment constraint (*i.e.* the deviation from the SM expectation) to our models with a positive  $\mu$ -term. In general it is not difficult to fulfill the  $a_\mu$  condition. Compared to figure 4 the results essentially do not change. In reference [90] we find the three most important MSSM loop contributions to  $a_\mu$ :

$$a_\mu(\widetilde{W} - \widetilde{H}, \widetilde{\nu}_\mu) = \frac{g^2}{8\pi^2} \frac{m_\mu^2 M_2 \mu \tan \beta}{m_{\widetilde{\nu}}^4} F_a \left( \frac{M_2^2}{m_{\widetilde{\nu}}^2}, \frac{\mu^2}{m_{\widetilde{\nu}}^2} \right), \quad (29)$$

$$a_\mu(\widetilde{B}, \widetilde{\mu}_L - \widetilde{\mu}_R) = \frac{g'^2}{8\pi^2} \frac{m_\mu^2 \mu \tan \beta}{M_1^3} F_b \left( \frac{m_{\widetilde{\mu}_L}^2}{M_1^2}, \frac{m_{\widetilde{\mu}_R}^2}{M_1^2} \right), \quad (30)$$

$$a_\mu(\widetilde{B} - \widetilde{H}, \widetilde{\mu}_R) = -\frac{g'^2}{8\pi^2} \frac{m_\mu^2 M_1 \mu \tan \beta}{m_{\widetilde{\mu}_R}^4} F_b \left( \frac{M_1^2}{m_{\widetilde{\mu}_R}^2}, \frac{\mu^2}{m_{\widetilde{\mu}_R}^2} \right). \quad (31)$$

Here, the positive defined functions  $F_a$  and  $F_b$  are given by:

$$\begin{aligned} F_a(x, y) &= -\frac{G_3(x) - G_3(y)}{x - y}, \\ F_b(x, y) &= -\frac{G_4(x) - G_4(y)}{x - y}, \\ G_3(x) &= \frac{1}{2(x-1)^3} [(x-1)(x-3) + 2 \ln x], \\ G_4(x) &= \frac{1}{2(x-1)^3} [(x-1)(x+1) - 2x \ln x]. \end{aligned}$$



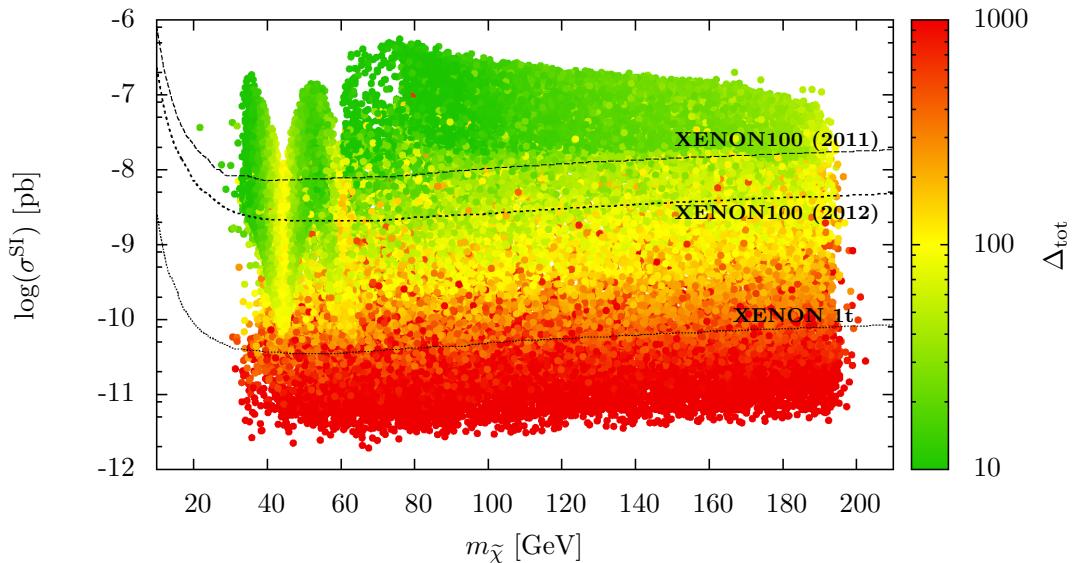


Figure 10: The level of fine-tuning after inclusion of the muon anomalous magnetic moment for positive values of the  $\mu$ -term.

It is commonly believed that  $a_\mu$  cannot be fulfilled for a negative  $\mu$ -term if  $M_1$  and  $M_2$  are positive [91]. However, if equation (31), the bino–higgsino–right-handed smuon loop, dominates over the sum of the other contributions, equation (29), the wino–higgsino–muon sneutrino loop, and equation (30), the bino–left-handed smuon–right-handed smuon loop, the total amount of the achieved positive pull of  $a_\mu$  can be sufficient to correctly deviate from the SM prediction. This situation occurs in the limit of  $m_{\tilde{l}_L}/m_{\tilde{l}_R} \gg 1$ , see left panel of figure 11. In this case the  $\tilde{\tau}_1$ 's are always light ( $\lesssim 400$  GeV) due to equation (18). It is very important to note that  $a_\mu$  is strongly dependent on the smuon parameters. Satisfying  $a_\mu$  becomes easier once one abandons the slepton mass generation universality since the relic density condition, which restricts the stau mass, would then become independent of  $a_\mu$ .

In our set-up we found that for large negative values of  $\mu$  the contributions of equations (29) and (30) become important again due to the behavior of the loop functions  $F_a$  and  $F_b$ . Because of the negative sign of  $\mu$  the pull of  $a_\mu$  tends to be toward negative values, out of the range that respects the experiments. We therefore find a lower limit on  $\mu$  of about -1500 GeV, see right panel of figure 11. This immediately favors low fine-tuned points as applying the  $a_\mu$  condition automatically cuts out large negative values of  $\mu$ . A great part of the models whose stau mass is strongly influenced by  $(A_\tau - \mu \tan \beta)$  drop out, and so do the highly fine-tuned scenarios from Higgs-resonant neutralino annihilation. Comparing to figure 2 one can see that a great part of the direct detection plane at low  $\sigma^{\text{SI}}$  is filled by slepton annihilation.

Taking a more restrictive limit for  $a_\mu$  at a  $2\sigma$  level we find an increase of the lower border on  $\mu$  and, related to this, a blank region in the direct detection plane at the  $Z$ -resonance (compare

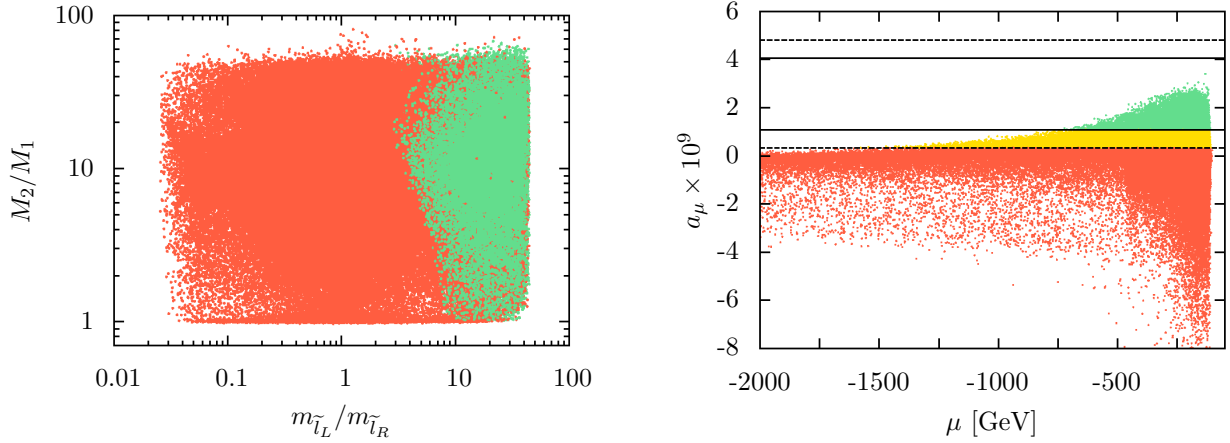


Figure 11: The left plot shows the  $a_\mu$  condition as a function of  $M_2/M_1$  and  $m_{\tilde{l}_L}/m_{\tilde{l}_R}$ . Only the green scenarios satisfy 3  $\sigma$  cut of the  $a_\mu$  condition.  $m_{\tilde{l}_L}/m_{\tilde{l}_R}$  must be much greater than one in order to respect  $a_\mu$  for a negative  $\mu$ -term. The right panel indicates the behavior of  $a_\mu$  when moving to smaller values of  $\mu$ . Green dots satisfy a 2  $\sigma$ , yellow dots a 3  $\sigma$  cut of  $a_\mu$ .

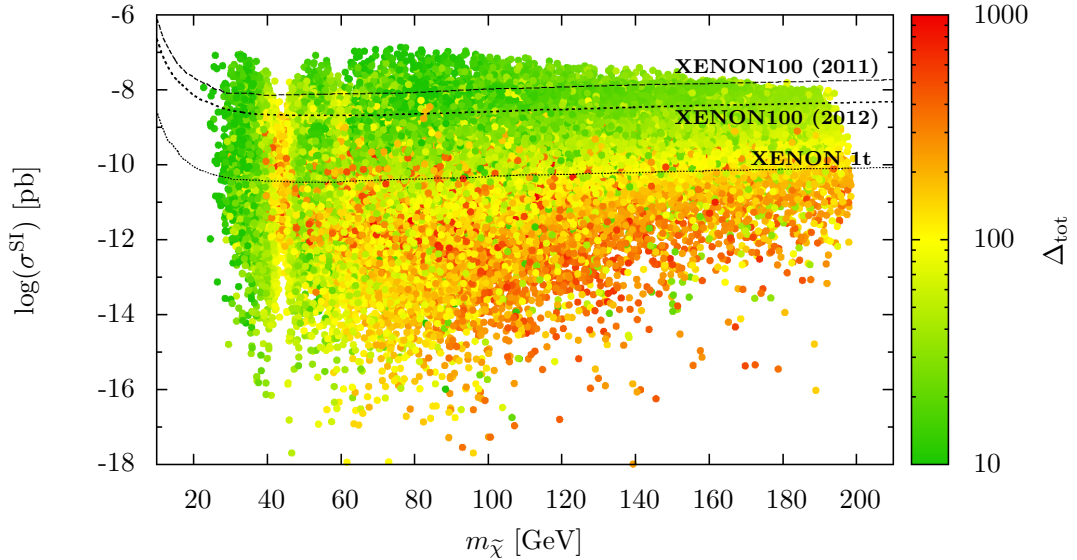


Figure 12: The level of fine-tuning after inclusion of the muon magnetic moment for a negative  $\mu$ -term in analogy to figure 10.

figure 13). As argued earlier, around this resonance a suppression of the neutralino-neutralino- $Z$ -coupling is necessary to satisfy the relic density condition. Because of the stronger constraint on  $\mu$

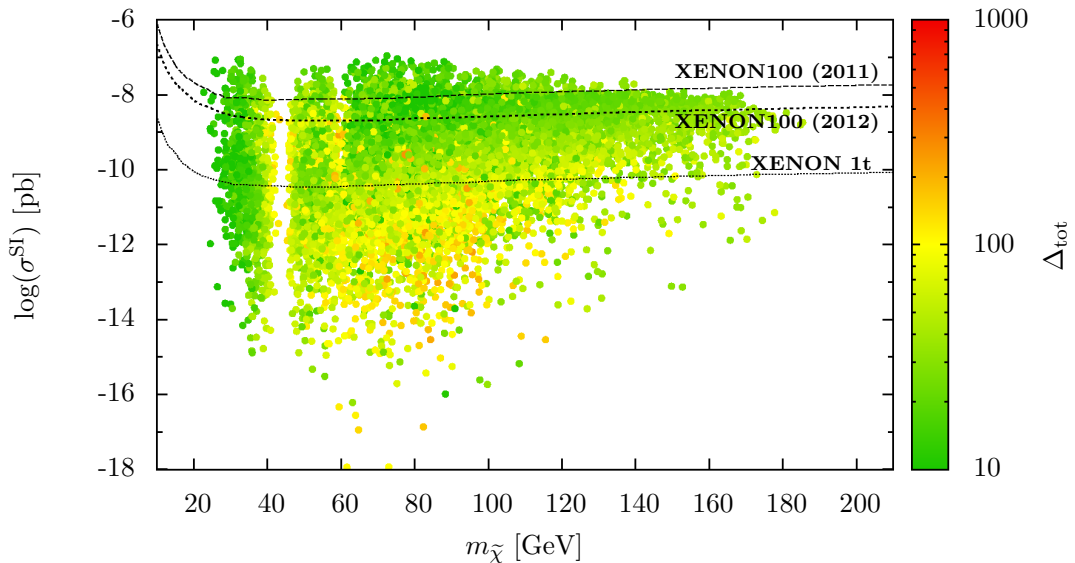


Figure 13: The level of fine-tuning after inclusion of the muon magnetic moment at a  $2\sigma$  level for a negative  $\mu$ -term in analogy to figure 10.

from the  $a_\mu$  limit, this suppression cannot be strong enough and the relic density condition fails to be fulfilled. Not only due to uncertainties of hadronic effects, but also as our essential results are not changed, we prefer to use the  $3\sigma$  limit on  $a_\mu$ .

The muon anomalous magnetic moment condition has no effect on the low fine-tuned models and, as argued above, less fine-tuned scenarios are even preferred (see figure 12). Note again, that in the mass range  $m_{\tilde{\chi}} \approx [60, 80]$  GeV neutralino annihilation can proceed via light staus to produce the correct relic abundance (compare figure 2 and references [21, 26, 28]). A great part of the parameter space with  $\Delta_{\text{tot}} \lesssim 100$  will be probed by future direct searches, but there are regions left that will not be tested.

We emphasize that a negative sign of  $\mu$  is by no mean in contradiction to the  $a_\mu$  condition even though we did not distinguish between slepton generations. Therefore, this case should be paid more attention to in future studies.

#### 4.5 The functional tuning of $\sigma^{\text{SI}}$

In section 4.3 we argued that the direct detection cross-section may become very small for a negative  $\mu$ -term if cancellations between the light and heavy Higgs contributions are almost exact. This is only possible when the wino component is negative, or equivalently, for positive  $M_1 + \mu \sin 2\beta$ . In other words: This depends in a very sensitive way on the functional dependence of  $\sigma^{\text{SI}}$  on this relation.

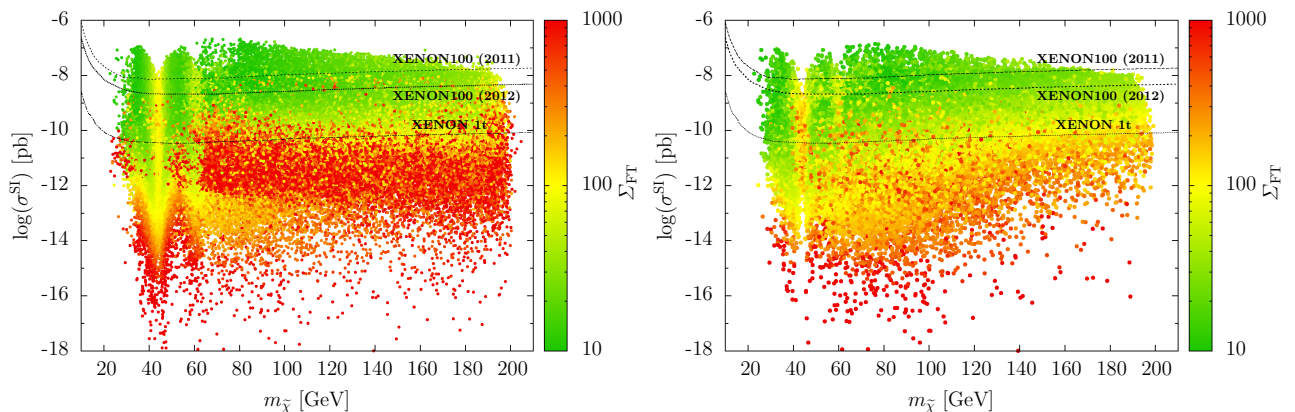


Figure 14: The distribution of the fine-tuning measure  $\Sigma_{\text{FT}}$ , that includes the functional tuning of  $\sigma^{\text{SI}}$  and the electroweak fine-tuning, in the direct detection plane for a negative  $\mu$ -term. The 3 sigma  $a_\mu$  constraint has been applied in the right panel.

To quantify these extremely accurate, tuned cancellations that might appear in  $\sigma^{\text{SI}}$ , we therefore define a functional fine-tuning,  $\Delta_f$ , analogously to equation (4):

$$\Delta f_i \equiv \left| \frac{\partial \ln \sigma^{\text{SI}}}{\partial \ln p_i} \right|, \quad \Delta_f \equiv \sqrt{\sum_{p_i=\mu, \tan \beta, M_1, M_2, m_A} \{\Delta f_i\}^2}. \quad (32)$$

The overall fine-tuning measure that includes both, the electroweak and the functional tuning, is then defined as:

$$\Sigma_{\text{FT}} \equiv \sqrt{\Delta_{\text{tot}}^2 + \Delta_f^2}. \quad (33)$$

In this way we deal with both tunings on equal footing.

In figure 14 we show how the overall fine-tuning measure,  $\Sigma_{\text{FT}}$ , maps into the direct detection plane. Of course, this measure only makes sense for a negative  $\mu$ -term since no cancellations are possible if  $\mu$  is positive. It is visible comparing to figure 12 that for those scenarios in which the cancellations suppress  $\sigma^{\text{SI}}$  below approximately  $10^{-14}$  pb the functional tuning measure becomes important and rises the overall tuning into an unacceptable range. For larger cross-sections the fine-tuning is still dominated by the sensitivity of the  $Z$ -mass and no change to the previously discussed results is observed. Comparing the left- and right-panel of figure 14 one can again observe the removal of the highly fine-tuned band containing models with light staus whose mass is strongly influenced by the off-diagonal stau mass matrix elements, when the  $a_\mu$  constraint is applied.

We see that even when the functional tuning measure is taken into account scenarios that possess a fine-tuning  $\Sigma_{\text{FT}}$  lower than 100 are possible in the pMSSM avoiding all of our applied constraints.

#### 4.6 The functional tuning of $\Omega h^2$

Analogously to the previous section one can also discuss a possible tuning of the relic abundance, as has been suggested in [49]. We again define the functional fine-tuning to be:

$$\Delta \tilde{f}_i \equiv \left| \frac{\partial \ln \Omega h^2}{\partial \ln p_i} \right|, \quad \Delta_{\tilde{f}} \equiv \sqrt{\sum_{p_i} \{\Delta \tilde{f}_i\}^2}, \quad (34)$$

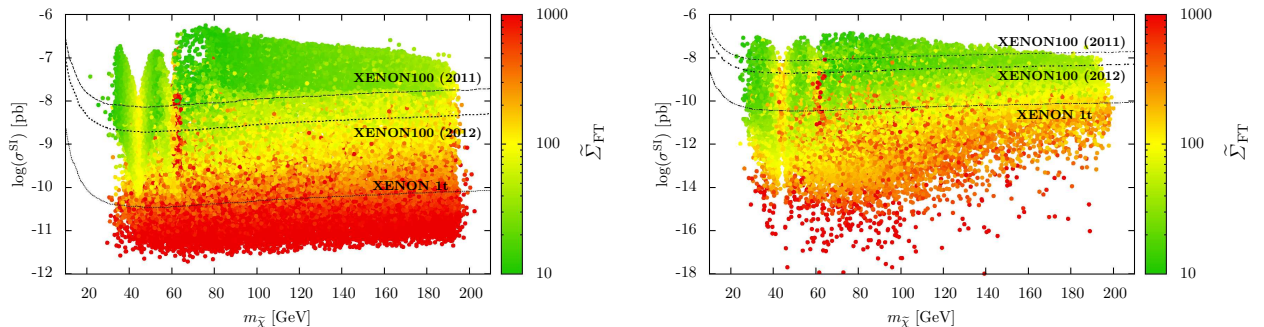


Figure 15: The distribution of the fine-tuning measure  $\tilde{\Sigma}_{\text{FT}}$  in the direct detection plane for a positive (left panel) and negative (right panel)  $\mu$ -term. The 3 sigma  $a_\mu$  constraint has been applied in both panels.

where the sum here runs over all eleven input parameters. The overall tuning is then given by:

$$\tilde{\Sigma}_{\text{FT}} \equiv \sqrt{\Delta_{\text{tot}}^2 + \Delta_{\text{f}}^2 + \Delta_{\text{f}}^2}. \quad (35)$$

Remember that for positive  $\mu$  we set  $\Delta_{\text{f}} = 0$  because there is no “accidental” cancellation. From our analysis and figure 15 we observe that the tuning of the relic density is generally low and plays a subdominant role compared to the electroweak tuning. The only tuned solutions occur close to the  $h$ -resonance. This is explained by the narrow decay width of the Higgs boson.

For a scenario to lie inside this narrow resonance and to produce the correct relic abundance, the parameters need to fulfill certain relations which leads to a high sensitivity of  $\Omega h^2$  at  $m_\chi \approx m_h/2$ . Such a tuning does not appear for a larger resonance as is the case for the  $Z$ -boson. Observe also, that, despite of the narrow Higgs decay width, the resonant region of light Higgs annihilation starts for Dark Matter masses much below  $m_h/2$  since the kinetic energy of the neutralino contributes to their overall energy (see section 4.2).

Even though not clearly visible for the negative  $\mu$  case in figure 15 (simply because the untuned scenarios where slepton annihilation is the most important annihilation mechanism outnumber the tuned scenarios) the effect is the same and independent of the sign of  $\mu$ .

#### 4.7 Parameter mapping distribution of our models

Throughout this paper we have so far studied how much tuning is required to reach a certain point in the  $m_{\tilde{\chi}} - \sigma^{\text{SI}}$  plane. In the end we would also like to briefly look at the mapping between model parameters and physical quantities, which does not play a role in the previous results. Within the MSSM it is clear that a statistical interpretation of the mapping of the model parameters to the  $m_{\tilde{\chi}} - \sigma^{\text{SI}}$  plane does not make sense, since there is only one solution in the end. But the mapping is nevertheless interesting if one thinks beyond, since it shows preferred physical regions in the  $m_{\tilde{\chi}} - \sigma^{\text{SI}}$  plane under the assumption that all model parameters have equal probability in an embedding which explains these parameters. This is shown in figure 16, where the color coding shows in addition the

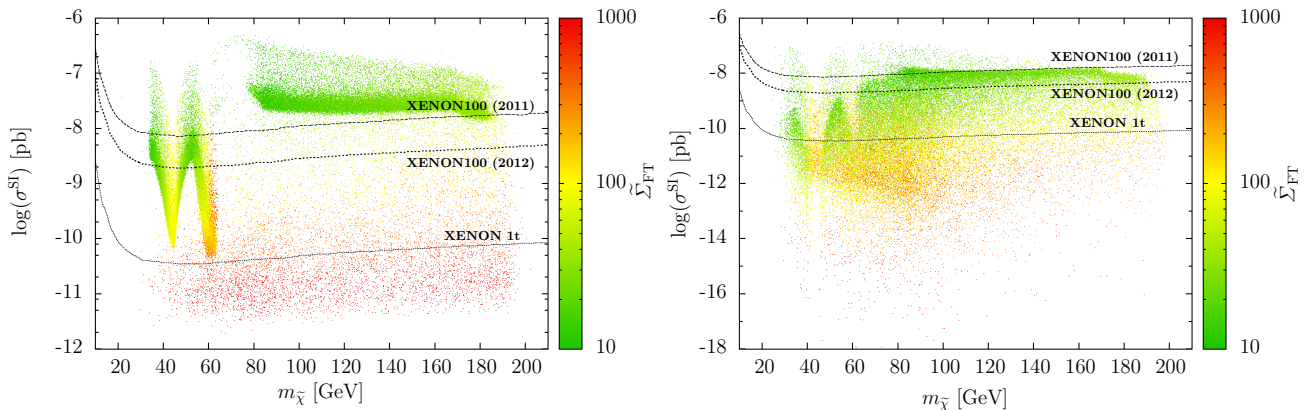


Figure 16: The level of fine-tuning and the density of model points arising from a homogeneously (randomized) scan of the parameter space. The case of  $\mu > 0$  is displayed in the left and  $\mu < 0$  in the right panel. All experimental constraints are taken into account including the muon anomalous magnetic moment.

previously discussed fine-tuning measure. It is immediately apparent that some regions are more densely populated. For example, we see that the regions from  $Z, h, H$  and  $A$  resonant annihilations and the light chargino mediated annihilation into  $W$ -bosons have a stronger weight than light stau annihilations for positive  $\mu$  (see left panel of figure 16). Note, that the light chargino and heavy and CP-odd Higgs annihilations have now been ruled out by the XENON100 (2012) update. For a negative  $\mu$ -term stau annihilations are also important, especially in the region  $m_{\tilde{\chi}} \in [65, 80]$  GeV. Signals from direct searches should be expected in the untuned, densely populated regions of the parameter space, which are not yet excluded by data (especially XENON100). However, we would like to stress again that such a mapping has no meaning within the MSSM and that the shown plots rest on the assumption of equal probability in some embedding.

## 5 Discussion and conclusions

In this paper we have analyzed the naturalness of neutralino Dark Matter in the non-universal gaugino model within the framework of the minimal supersymmetric extension of the Standard Model. We have taken into account all cosmological (upper and lower bound on the relic density), collider and flavor constraints including the results of XENON100 (2012), LHC data on the Higgs mass,  $\text{Br}(B_s \rightarrow \mu^+ \mu^-)$  and pseudo-Higgs searches. Hereby the soft supersymmetry breaking terms are parameterized by 11 independent free parameters, that we have chosen such that the lightest supersymmetric particle is the lightest neutralino with a mass smaller than 200 GeV. We studied from the Dark Matter perspective how much fine-tuning is needed to reach a certain point in the  $m_{\tilde{\chi}} - \sigma^{\text{SI}}$  plane. Therefore we use a parameter fine-tuning measure (see equation (4)) which was used before in order to study the naturalness of the Higgs – SUSY breaking scale separation.

We first presented in figure 1 the contribution to the Dark Matter abundance  $\Omega h^2$  for different annihilation mechanisms as a function of  $m_{\tilde{\chi}}$ . Demanding that neutralinos provide the right amount of Dark Matter, we restrict the further scans to cases where  $\Omega h^2 \in [0.089, 0.136]$ .

We also investigated the dominant neutralino annihilation mechanisms (figure 1) and have shown their arrangement in the  $m_{\tilde{\chi}} - \sigma^{\text{SI}}$ -plane (figure 2). In case of a signal in a direct detection experiment the most important annihilation mechanism can be deduced and we would know which channel at the LHC is promising for production of neutralino Dark Matter. To avoid the limits of the direct detection results of XENON100 (2012), we showed that light stau annihilation of neutralinos in the early Universe play a special role, not only in the mass range of light neutralinos,  $\lesssim 30$  GeV, but also between  $\simeq [60, 80]$  GeV, which has been missed so far in other studies. It is important to differently parameterize the soft SUSY masses of the left- ( $m_{\tilde{t}_L}$ ) and right-handed ( $m_{\tilde{t}_R}$ ) sleptons.

Note that we scanned the input parameter space in such a way that we obtain the fine-tuning for every point in the  $m_{\tilde{\chi}} - \sigma^{\text{SI}}$  plane which is accessible. This implies that the density of points has no meaning, but that the envelope implies that certain areas cannot be reached by any input parameter. With this method we showed in figure 4 how the electroweak fine-tuning maps into the direct detection plane and found that a great part of untuned regions is already excluded by the current XENON100 (2012) limit when the supersymmetric Higgs mass parameter, the  $\mu$ -term, is positive. A general trend for higher fine-tuning for smaller  $\sigma^{\text{SI}}$  is then visible. This trend can easily be understood, since the cross-section departs more and more from its natural value set by the generic scale. Thus, future direct detection experiments will push the amount of the electroweak fine-tuning further up. The only exception occurs for neutralino masses that allow for resonant annihilations, especially near the  $Z$ - and  $h$ -boson resonances.

This last statement is also valid for a negative  $\mu$ -term and the electroweak fine-tuning near the  $Z$ - and  $h$ -resonance stays small independent of the value of  $\sigma^{\text{SI}}$ . Additionally, due to cancellations between contributions from light and heavy Higgs exchanges the direct detection cross-section gets shifted to smaller values, such that the XENON100 (2012) exclusion limit is fulfilled easily. A negative  $\mu$ -term is therefore favored from a fine-tuning perspective (see figure 6).

In our analytical study (see figure 9) we have discussed the reason why the negative value of the  $\mu$ -term allows for these cancellations in the spin-independent cross-section, and showed that the combination of input parameters ( $M_1 + \mu \sin 2\beta$ ) and the sign of the wino component are responsible for decreasing  $\sigma^{\text{SI}}$  to values that can be as low as  $10^{-20}$  pb (see also figure 6). Since these cancellations might be viewed as an instance of tuning, we reevaluated the fine-tuning by adding a measure of “equation-tuning” and found that scenarios with  $\sigma^{\text{SI}} \lesssim 10^{-15}$  pb are always unbearably tuned (figure 14). We find the scenario with the lowest fine-tuning, independent of the sign of  $\mu$ , at  $m_{\tilde{\chi}} \approx 84$  GeV and  $\sigma^{\text{SI}} \approx 2.0 \times 10^{-9}$  pb just below the new limit.

Even for a negative  $\mu$ -term we were able to get the correct positive pull for the muon anomalous magnetic moment,  $a_\mu$ , to correctly deviate from the Standard Model (figure 11). This has been thought to be very difficult, but is possible due to the bino–higgsino–right-handed smuon loop which contributes to  $a_\mu$  dominantly when both gaugino masses are positive ( $M_1 > 0$  and  $M_2 > 0$ ) and  $m_{\tilde{t}_L} \gg m_{\tilde{t}_R}$ . If the latter condition is fulfilled staus are generally light ( $\lesssim 400$  GeV) and help to respect the cosmological abundance of Dark Matter by light stau annihilation in the complete mass region of the neutralino. It should be stressed that there is an easy way to satisfy  $a_\mu$ , namely, if additional parameters for the smuon masses, *i.e.*  $m_{\tilde{\mu}_{L,R}}$ , are introduced. In this case we can avoid the connection between the relic density and the anomalous muon magnetic moment and fulfill both conditions without any doubt. Therefore, the case of a negative sign of the  $\mu$ -term is equally important and should be investigated more carefully in future studies.

Note that the density of points is meaningless except in figure 16, since we do not assign a probability measure, but determine only the amount of tuning required to reach a certain point

in the  $m_{\tilde{\chi}} - \sigma^{\text{SI}}$  plane. The envelope implies, however, that these points cannot be reached. In this context it is interesting to note that the cross-section of the neutralino annihilating into two photons and into a pair of photon and  $Z$ -boson is loop suppressed and is therefore much smaller than the requirement from the claimed 130 GeV gamma-ray line in the Fermi-LAT data. Thus, our models can not explain this “evidence”. Besides, very light neutralino scenarios consistent with the DAMA/LIBRA, CoGeNT, CRESST experiments cannot be explained in the pMSSM especially due to the limits on  $\text{Br}(B_s \rightarrow \mu^+ \mu^-)$  and on the pseudo-Higgs mass-tan  $\beta$ -plane.

Finally, in section 4.7 we have discussed in addition the parameter mapping distribution of our models into the  $m_{\tilde{\chi}} - \sigma^{\text{SI}}$  plane (figure 16). We found that the  $Z$ - and  $h$ -boson resonant areas become the preferred regions to detect neutralino dark matter if the  $\mu$ -term is positive. For negative  $\mu$  another important region is formed by light stau annihilation, that has avoided direct searches so far.

Note that taking into account the branching ratio of the decay  $B_s \rightarrow \mu^+ \mu^-$  [92] does not change our discussion and results because we are in the decoupling regime and  $\tan \beta$  is not too high. There are only few models that do not satisfy the lower limit of  $\text{Br}(B_s \rightarrow \mu^+ \mu^-)$  at 95 % C.L. Furthermore, the strong bounds from LHC for light generation squarks and gluino masses [93] do not affect the main conclusion of our discussions, since its contributions to the direct detection and pair-(co)annihilation cross-sections are typically subdominant.

Note added: After the completion of this work, two papers appeared which have studied the importance of the  $\mu$ -term sign for the direct detection cross-section within the frame work of MSSM [94] and NMSSM [95], respectively. In section 4.3 we have discussed the suppression of  $\sigma^{\text{SI}}$  in the region (so-called “blind spot”) where a particular combination of SUSY parameter  $M_1 + \mu \sin 2\beta$  is small.

## Acknowledgments

One of us (Y. T.) wishes to thank L. Calibbi and T. Ota for collaboration in early stages of the project and useful discussions. The work of Y. T. is supported by the ERC Starting Grant MANITOP.



## References

- [1] E. Aprile, “Latest XENON100 Results”, Talk given at Dark Attack 2012, 18 July 2012, Ascona, Switzerland
- [2] F. Gianotti, “Status of Standard Model Higgs searches in ATLAS”, at Latest update in the search for the Higgs boson, 4 July 2012, CERN, Geneva, Switzerland.
- [3] J. Incandela, “Status of Standard Model Higgs searches in CMS”, at Latest update in the search for the Higgs boson, 4 July 2012, CERN, Geneva, Switzerland.
- [4] J. R. Ellis, G. Ridolfi and F. Zwirner, Phys. Lett. B **257** (1991) 83.
- [5] J. R. Ellis, G. Ridolfi and F. Zwirner, Phys. Lett. B **262** (1991) 477.
- [6] Y. Okada, M. Yamaguchi and T. Yanagida, Prog. Theor. Phys. **85** (1991) 1.
- [7] H. E. Haber and R. Hempfling, Phys. Rev. Lett. **66** (1991) 1815.
- [8] M. Drees and M. M. Nojiri, Phys. Rev. D **45** (1992) 2482.
- [9] G. Degrassi, S. Heinemeyer, W. Hollik, P. Slavich and G. Weiglein, Eur. Phys. J. C **28** (2003) 133 [hep-ph/0212020].
- [10] O. Buchmueller, R. Cavanaugh, A. De Roeck, J. R. Ellis, H. Flacher, S. Heinemeyer, G. Isidori and K. A. Olive *et al.*, Eur. Phys. J. C **64** (2009) 391 [arXiv:0907.5568 [hep-ph]].
- [11] E. Komatsu *et al.* [WMAP Collaboration], Astrophys. J. Suppl. **192** (2011) 18 [arXiv:1001.4538 [astro-ph.CO]].
- [12] H. Goldberg, Phys. Rev. Lett. **50** (1983) 1419 [Erratum-ibid. **103** (2009) 099905].
- [13] J. R. Ellis, J. S. Hagelin, D. V. Nanopoulos, K. A. Olive and M. Srednicki, Nucl. Phys. B **238** (1984) 453.
- [14] G. Jungman, M. Kamionkowski and K. Griest, Phys. Rept. **267** (1996) 195 [hep-ph/9506380].
- [15] L. Bergström, Rept. Prog. Phys. **63** (2000) 793 [hep-ph/0002126].
- [16] H. P. Nilles, Phys. Rept. **110** (1984) 1.
- [17] H. E. Haber and G. L. Kane, Phys. Rept. **117** (1985) 75.
- [18] S. P. Martin, “A Supersymmetry primer”, hep-ph/9709356.
- [19] J. R. Ellis, K. Enqvist, D. V. Nanopoulos and F. Zwirner, Mod. Phys. Lett. A **1** (1986) 57.
- [20] R. Barbieri and G. F. Giudice, Nucl. Phys. B **306** (1988) 63.
- [21] M. Farina, M. Kadastik, D. Pappadopulo, J. Pata, M. Raidal and A. Strumia, Nucl. Phys. B **853** (2011) 607 [arXiv:1104.3572 [hep-ph]].
- [22] O. Buchmueller, R. Cavanaugh, A. De Roeck, M. J. Dolan, J. R. Ellis, H. Flacher, S. Heinemeyer and G. Isidori *et al.*, Eur. Phys. J. C **72** (2012) 1878 [arXiv:1110.3568 [hep-ph]].

- [23] O. Buchmueller, R. Cavanaugh, A. De Roeck, M. J. Dolan, J. R. Ellis, H. Flacher, S. Heinemeyer and G. Isidori *et al.*, arXiv:1112.3564 [hep-ph].
- [24] S. S. AbdusSalam, B. C. Allanach, F. Quevedo, F. Feroz and M. Hobson, Phys. Rev. D **81** (2010) 095012 [arXiv:0904.2548 [hep-ph]].
- [25] S. Sekmen, S. Kraml, J. Lykken, F. Moortgat, S. Padhi, L. Pape, M. Pierini and H. B. Prosper *et al.*, JHEP **1202** (2012) 075 [arXiv:1109.5119 [hep-ph]].
- [26] A. Arbey, M. Battaglia and F. Mahmoudi, Eur. Phys. J. C **72** (2012) 1847 [arXiv:1110.3726 [hep-ph]].
- [27] D. Albornoz Vásquez, G. Bélanger, J. Billard and F. Mayet, Phys. Rev. D **85** (2012) 055023 [arXiv:1201.6150 [hep-ph]].
- [28] M. W. Cahill-Rowley, J. L. Hewett, A. Ismail and T. G. Rizzo, arXiv:1206.5800 [hep-ph].
- [29] R. Bernabei *et al.* [DAMA and LIBRA Collaborations], Eur. Phys. J. C **67** (2010) 39 [arXiv:1002.1028 [astro-ph.GA]].
- [30] C. E. Aalseth *et al.* [CoGeNT Collaboration], Phys. Rev. Lett. **106** (2011) 131301 [arXiv:1002.4703 [astro-ph.CO]].
- [31] D. Hooper and T. Plehn, Phys. Lett. B **562** (2003) 18 [hep-ph/0212226].
- [32] A. Bottino, N. Fornengo and S. Scopel, Phys. Rev. D **67** (2003) 063519 [hep-ph/0212379].
- [33] H. K. Dreiner, S. Heinemeyer, O. Kittel, U. Langenfeld, A. M. Weber and G. Weiglein, Eur. Phys. J. C **62** (2009) 547 [arXiv:0901.3485 [hep-ph]].
- [34] E. Kuflik, A. Pierce and K. M. Zurek, Phys. Rev. D **81** (2010) 111701 [arXiv:1003.0682 [hep-ph]].
- [35] D. Feldman, Z. Liu and P. Nath, Phys. Rev. D **81** (2010) 117701 [arXiv:1003.0437 [hep-ph]].
- [36] D. A. Vásquez, G. Bélanger, C. Boehm, A. Pukhov and J. Silk, Phys. Rev. D **82** (2010) 115027 [arXiv:1009.4380 [hep-ph]].
- [37] N. Fornengo, S. Scopel and A. Bottino, Phys. Rev. D **83** (2011) 015001 [arXiv:1011.4743 [hep-ph]].
- [38] L. Calibbi, T. Ota and Y. Takanishi, JHEP **1107** (2011) 013 [arXiv:1104.1134 [hep-ph]].
- [39] A. Arbey, M. Battaglia and F. Mahmoudi, arXiv:1205.2557 [hep-ph].
- [40] G. Angloher, M. Bauer, I. Bavykina, A. Bento, C. Bucci, C. Ciemniak, G. Deuter and F. von Feilitzsch *et al.*, Eur. Phys. J. C **72** (2012) 1971 [arXiv:1109.0702 [astro-ph.CO]].
- [41] L. Calibbi, T. Ota and Y. Takanishi, arXiv:1112.0219 [hep-ph].
- [42] J. Kopp, T. Schwetz and J. Zupan, JCAP **1203** (2012) 001 [arXiv:1110.2721 [hep-ph]].
- [43] E. Aprile *et al.* [XENON100 Collaboration], Phys. Rev. Lett. **107** (2011) 131302 [arXiv:1104.2549 [astro-ph.CO]].

- [44] E. Aprile *et al.* [XENON100 Collaboration], Phys. Rev. Lett. **105** (2010) 131302 [arXiv:1005.0380 [astro-ph.CO]].
- [45] J. Angle *et al.* [XENON Collaboration], Phys. Rev. Lett. **100** (2008) 021303 [arXiv:0706.0039 [astro-ph]].
- [46] Z. Ahmed *et al.* [CDMS-II Collaboration], Phys. Rev. Lett. **106** (2011) 131302 [arXiv:1011.2482 [astro-ph.CO]].
- [47] M. Perelstein and C. Spethmann, JHEP **0704** (2007) 070 [hep-ph/0702038].
- [48] L. J. Hall, D. Pinner and J. T. Ruderman, JHEP **1204**, 131 (2012) [arXiv:1112.2703 [hep-ph]].
- [49] J. R. Ellis and K. A. Olive, Phys. Lett. B **514** (2001) 114 [hep-ph/0105004].
- [50] R. Kitano and Y. Nomura, Phys. Rev. D **73** (2006) 095004 [hep-ph/0602096].
- [51] S. Cassel, D. M. Ghilencea and G. G. Ross, Nucl. Phys. B **835** (2010) 110 [arXiv:1001.3884 [hep-ph]].
- [52] D. M. Ghilencea, H. M. Lee and M. Park, arXiv:1203.0569 [hep-ph].
- [53] M. Perelstein and B. Shakya, JHEP **1110** (2011) 142 [arXiv:1107.5048 [hep-ph]].
- [54] D. Albornoz Vásquez, G. Bélanger and C. Boehm, Phys. Rev. D **84** (2011) 095015 [arXiv:1108.1338 [hep-ph]].
- [55] M. Matsumoto and T. Nishimura, “Mersenne Twister: a 623-dimensionally equidistributed uniform pseudorandom number generator”, ACM Transactions on Modeling and Computer Simulation **8** (1998) 3.
- [56] T. Nishimura, “Tables of 64-bit Mersenne Twisters”, ACM Transactions on Modeling and Computer Simulation **10** (2000) 348.
- [57] B. Dumont, G. Bélanger, S. Fichet, S. Kraml and T. Schwetz, arXiv:1206.1521 [hep-ph].
- [58] G. Aad *et al.* [ATLAS Collaboration], Phys. Lett. B **710** (2012) 49 [arXiv:1202.1408 [hep-ex]].
- [59] S. Chatrchyan *et al.* [CMS Collaboration], Phys. Lett. B **710** (2012) 26 [arXiv:1202.1488 [hep-ex]].
- [60] G. Aad *et al.* [ATLAS Collaboration], Phys. Rev. Lett. **108** (2012) 111803 [arXiv:1202.1414 [hep-ex]].
- [61] S. Chatrchyan *et al.* [CMS Collaboration], Phys. Lett. B **710** (2012) 403 [arXiv:1202.1487 [hep-ex]].
- [62] ATLAS Collaboration, “An update to the combined search for the Standard Model Higgs boson with the ATLAS detector at the LHC using up to  $4.9 \text{ fb}^{-1}$  of  $pp$  collision data at  $\sqrt{s} = 7 \text{ TeV}$ ”, ATLAS-CONF-2012-019.
- [63] CMS Collaboration, “Combined results of searches for a Higgs boson in the context of the standard model and beyond-standard models”, CMS-PAS-HIG-12-008.

- [64] E. Barberio *et al.* [Heavy Flavor Averaging Group Collaboration], arXiv:0808.1297 [hep-ex].
- [65] R. Aaij *et al.* [LHCb Collaboration], arXiv:1203.4493 [hep-ex].
- [66] D. Asner *et al.* [Heavy Flavor Averaging Group Collaboration], arXiv:1010.1589 [hep-ex].
- [67] M. Antonelli *et al.* [FlaviaNet Working Group on Kaon Decays Collaboration], arXiv:0801.1817 [hep-ph].
- [68] G. W. Bennett *et al.* [Muon G-2 Collaboration], Phys. Rev. D **73** (2006) 072003 [hep-ex/0602035].
- [69] [ALEPH and DELPHI and L3 and OPAL and SLD and LEP Electroweak Working Group and SLD Electroweak Group and SLD Heavy Flavour Group Collaborations], Phys. Rept. **427** (2006) 257 [hep-ex/0509008].
- [70] G. Aad *et al.* [ATLAS Collaboration], Phys. Lett. B **710** (2012) 67 [arXiv:1109.6572 [hep-ex]].
- [71] S. Chatrchyan *et al.* [CMS Collaboration], Phys. Rev. Lett. **107** (2011) 221804 [arXiv:1109.2352 [hep-ex]].
- [72] G. Aad *et al.* [ATLAS Collaboration], “Search for squarks and gluinos with the ATLAS detector using final states with jets and missing transverse momentum and 4.7 fb<sup>-1</sup> of  $\sqrt{s} = 7$  TeV proton-proton collision data”, ATLAS-CONF-2012-033.
- [73] A. Parker, “SUSY Searches (ATLAS/CMS): the Lady Vanishes”, ICHEP 2012, 4-11 July 2012, Melbourne, Australia.
- [74] G. Aad *et al.* [ATLAS Collaboration], Phys. Lett. B **705** (2011) 174 [arXiv:1107.5003 [hep-ex]].
- [75] S. Chatrchyan *et al.* [CMS Collaboration], Phys. Lett. B **713** (2012) 68 [arXiv:1202.4083 [hep-ex]].
- [76] G. Abbiendi *et al.* [OPAL Collaboration], Eur. Phys. J. **C35** (2004) 1 [hep-ex/0401026].
- [77] K. Nakamura *et al.* [Particle Data Group Collaboration], J. Phys. G **37** (2010) 075021.
- [78] A. Djouadi, J.-L. Kneur and G. Moultaka, Comput. Phys. Commun. **176** (2007) 426 [hep-ph/0211331].
- [79] G. Bélanger, F. Boudjema, A. Pukhov and A. Semenov, Comput. Phys. Commun. **176** (2007) 367 [hep-ph/0607059].
- [80] G. Bélanger, F. Boudjema, P. Brun, A. Pukhov, S. Rosier-Lees, P. Salati and A. Semenov, Comput. Phys. Commun. **182** (2011) 842 [arXiv:1004.1092 [hep-ph]].
- [81] F. Mahmoudi, Comput. Phys. Commun. **180** (2009) 1579 [arXiv:0808.3144 [hep-ph]].
- [82] G. Bélanger, F. Boudjema, A. Pukhov and A. Semenov, Comput. Phys. Commun. **180** (2009) 747 [arXiv:0803.2360 [hep-ph]].
- [83] C. Weniger, arXiv:1204.2797 [hep-ph].
- [84] T. Nihei, L. Roszkowski and R. Ruiz de Austri, JHEP **0203** (2002) 031 [hep-ph/0202009].

- [85] H. K. Dreiner, J. S. Kim and O. Lebedev, arXiv:1206.3096 [hep-ph].
- [86] T. Falk, A. Ferstl and K. A. Olive, Phys. Rev. D **59** (1999) 055009 [Erratum-ibid. D **60** (1999) 119904] [hep-ph/9806413].
- [87] A. Bottino, F. Donato, N. Fornengo and S. Scopel, Phys. Rev. D **59** (1999) 095003 [hep-ph/9808456].
- [88] S. Y. Choi, J. Kalinowski, G. A. Moortgat-Pick and P. M. Zerwas, Eur. Phys. J. C **22** (2001) 563 [Addendum-ibid. C **23** (2002) 769] [hep-ph/0108117].
- [89] R. Kitano and Y. Nomura, hep-ph/0606134.
- [90] G.-C. Cho, K. Hagiwara, Y. Matsumoto and D. Nomura, JHEP **1111** (2011) 068 [arXiv:1104.1769 [hep-ph]].
- [91] Y. G. Kim, T. Nihei, L. Roszkowski and R. Ruiz de Austri, JHEP **0212** (2002) 034 [hep-ph/0208069].
- [92] R. Aaij *et al.* [LHCb Collaboration], arXiv:1211.2674 [hep-ex].
- [93] G. Aad *et al.* [ATLAS Collaboration], Phys. Rev. D **87** (2013) 012008 [arXiv:1208.0949 [hep-ex]]; ATLAS-CONF-2013-007.
- [94] C. Cheung, L. J. Hall, D. Pinner and J. T. Ruderman, arXiv:1211.4873 [hep-ph].
- [95] M. Perelstein and B. Shakya, arXiv:1208.0833 [hep-ph].